Climatic and glacial impact on erosion patterns and sediment provenance in the Himalayan rain shadow, Zanskar River, NW India

Tara N. Jonell[1*], Andrew Carter[2], Philipp Böning[3], Katharina Pahnke[3], and Peter D. Clift[1,4],

[1]Department of Geology and Geophysics, Louisiana State University, Baton Rouge, LA 70803, USA

[2]Department of Earth and Planetary Sciences, Birkbeck College, London, WC1E 7HX, United Kingdom

[3]Max Planck Research Group for Marine Isotope Geochemistry, Institute for Chemistry and Biology of the Marine Environment (ICBM), University of Oldenburg, 26129 Oldenburg, Germany

[4]School of Geography Science, Nanjing Normal University, Nanjing 210023, China

ABSTRACT

Erosion is a key step in the destruction and recycling of the continental crust yet its primary drivers continue to be debated. The relative balance between climatic and solid Earth

forces in determining erosion patterns and rates, and in turn orogenic architecture, is unresolved. The monsoon-dominated frontal Himalaya is a classic example of how surface processes may drive focused denudation and potentially control structural evolution. We investigate whether there is a clear relationship between climate and erosion in the drier Himalayan rain shadow of northwest India where a coupled climate-erosion relationship is less clear. We present a new integrated dataset combining bulk petrography, geomorphometric analysis, detrital U-Pb zircon geochronology, and bulk Nd and Sr isotope geochemistry from modern river sediments that provides constraints on spatial patterns of sediment production and transport in the Zanskar River. Zanskar River sands are dominated by Greater Himalayan detritus sourced from the glaciated Stod River catchment that represents only 13% of the total basin area. Prevalent zircon peaks from the Cambro-Ordovician (440–500 Ma) and Mississippian-Permian (245–380 Ma) indicate more abundant pre-Himalayan granitoids in the northwest Himalaya than in the central and eastern Himalaya. Erosion from the widely-exposed Tethyan Himalaya, however, appears modest. Spatial patterns of erosion do not correlate with highest channel steepness. Our data demonstrate that Zanskar differs from the monsoon-soaked frontal Himalaya and the arid, extremely slow-eroding orogenic interior in that focused erosion and sediment production are driven by glaciers. Subsequent remobilization of glacially-derived sediments is likely controlled by monsoonal rainfall and we suggest sediment reworking plays an important role. These data support strong climatic control on modern orogenic erosion on the periphery of the Himalayan rain shadow.

INTRODUCTION

The growth and destruction of orogenic systems are governed by the distribution and pace of tectonically driven rock uplift and surface processes. Solid Earth and climatic forces together facilitate denudation that in turn regulates the flux and composition of sediments recycled through rivers to the oceans. How the magnitude of these forces and their resultant erosion shape orogens is debated. Many studies argue for strongly linked climate-precipitation and focused erosion (e.g., Beaumont et al., 2001; Clift et al., 2008; Hodges et al., 2004; Kirby and Ouimet, 2011; Thiede et al., 2004) while others favor a decisive solid Earth control (Burbank et al., 2003; Wallis et al., 2016). Constraining the roles of these processes is crucial in quantifying how sedimentation reflects tectonic and climatic conditions. If we are to relate exhumation and paleoenvironmental histories from long denuded mountain belts then analysis of the sedimentary record provides the only method to reconstruct these processes in relative continuity over long periods of geologic time.

The dramatic topographic and climatic gradients of the Himalaya-Tibetan orogen provide the opportunity to assess the interdependency between tectonics, climate, and surface processes. Intense summer monsoonal rainfall on the southern flank of the Himalaya produces extreme erosion, steep topographic relief (Bookhagen and Burbank, 2006; Bookhagen et al., 2005b; Gabet et al., 2008) and some of the highest riverine fluxes of sediment to the ocean (Milliman and Meade, 1983). Erosion patterns in river basins across the wet, frontal Himalaya, like the Marsyandi (e.g, Attal and Lavé, 2006; Garzanti et al., 2007), Sutlej (Bookhagen and Burbank, 2006), and Alaknanda Rivers (Srivastava et al., 2008) tightly correlate with the distribution and intensity of monsoon precipitation (Fig. 1). Moreover, focused erosion on the Himalayan front has been proposed to control the distribution of deep exhumation and tectonic strain (e.g, Beaumont et al., 2001; Thiede et al., 2004).

How erosion is facilitated by climatic processes is less clear farther north in the Himalayan rain shadow, where high topography impedes northward advection of monsoonal moisture onto the Tibetan Plateau. Arid regions north of the Indus River in Ladakh and the Karakorum show exhumation rates scale with tectonically generated topography and glacial cover rather than with precipitation as found along the Himalayan front (Dortch et al., 2011a; Munack et al., 2014; Wallis et al., 2016). Despite this apparent lack of correlation between precipitation and erosion, some observations suggest the Himalayan rain shadow may be especially sensitive to climatic perturbations. Intense summer rainstorms have resulted in modern day examples of extreme erosion (i.e., (Hobley et al., 2012) and suggest that volumetrically large sediment signals (>60% total flux) can be produced by only a few events (Bookhagen et al., 2005a; Wulf et al., 2010; Wulf et al., 2012). However, whether this is geologically important was questioned by Munack et al. (2014) who showed that the long-term denudation derived from ^{10}Be cosmogenic isotopes is consistent amongst samples both before and after the intensive climatic events of the summer 2010 in Ladakh.

Here we examine whether precipitation, glaciation, or rock uplift dominate in controlling modern erosion on the western margin of the Tibetan Plateau in the Zanskar River basin. This river is ideally situated for evaluating coupling between climate and erosion because it is the largest river basin in the Himalayan rain shadow draining the High Himalaya towards the north, directly into the trunk Indus River. Our investigation sets out to quantify sediment provenance in the Zanskar River basin to establish the modern relative spatial distributions of erosion, or erosion patterns. We further explore whether climate modulates sediment production and transport in the rain shadow as it does in the frontal ranges, or if present-day erosion instead reflects strong, underlying tectonic control.

BACKGROUND

Climatic and Geographic Setting

The Zanskar River basin lies directly north of the Himalayan topographic divide on the southern edge of the Tibetan Plateau and occupies a modern drainage area of 14,939 km^2 (Fig. 1). All material sourced from the Zanskar River basin transmits to the Indus River, the main river system routing water and sediment from the western Himalaya into the Arabian Sea for roughly the last ~45 m.y. (Clift et al., 2001). The broader Zanskar River basin can be subdivided into five catchments of the main tributaries: the Tsarap, Stod, Khurna, Markha, and Oma Rivers (Fig. 1C).

Glaciers occupy 8% of the Zanskar River basin, with some glacial tongues extending as low as ~4100 m (Owen, 2011; Taylor and Mitchell, 2000). Recessional and terminal moraines are preserved throughout Zanskar. Although glaciers were not much more widespread at the Last Glacial Maximum (~20 ka), older glaciations were quite extensive (Dortch et al., 2011a; Dortch et al., 2013; Hedrick et al., 2011; Owen et al., 2005). One terminal moraine dated to ~78 ka extended as low as ~3400 m to create the Padum Basin, which is a key confluence within the Zanskar catchment (Owen et al., 2002; Taylor and Mitchell, 2000).

Precipitation is delivered by the Summer Monsoon and Winter Western Disturbances (Westerlies) as rainfall in the summer (Jun–Aug) and snowfall in the winter, respectively (Owen and Benn, 2005). Dramatic attenuation of monsoonal precipitation across the topographic barrier of the High Himalaya produces a rain shadow to the north in the orogenic interior (Fig. 2). Likewise, a gradient is observed for Westerly-derived precipitation that decreases considerably to the southeast across this region (Leipe et al., 2014). Sutlej River basin weather station and hydrologic modelling data imply that 30–50% of the total annual precipitation to upper Indus

River tributaries is received as winter snowfall, and contributes as much as ~66% of the total yearly discharge as snow or glacial meltwater (Bookhagen and Burbank, 2010; Burbank et al., 2012).

Modern erosion rates in the frontal Himalaya are tightly coupled with monsoonal rainfall and discharge (e.g., Bookhagen, 2010; Gabet et al., 2008; Goodbred, 2003). Overall annual sediment fluxes from arid rain shadow regions, like the drier upper drainages of the Indus, Sutlej, and Marsyandi River basins (Fig. 1B), are lower because of lower runoff. In the upper Marsyandi and Sutlej Rivers, highest suspended sediment yields occur during late summer when temperatures are highest rather than at the onset of monsoon season (Burbank et al., 2012; Wulf et al., 2012). This suggests that subglacial drainage channels provide the initial flux, with progressively increasing contributions from hillslopes and river channels as summer monsoon rainfall arrives (e.g., Bookhagen and Burbank, 2010). Despite lower annual precipitation, high intensity monsoonal rainstorms can produce extreme erosion and, in only a few events, produce 30–50% of the total annual sediment flux in semi-arid to arid regions (Wulf et al., 2010; Wulf et al., 2012). These observations suggest, that at least under modern day climatic conditions, regions directly adjacent to the present rainfall maxima shadow potentially produce disproportionate sediment signals during such events (Bookhagen, 2010).

Geologic Setting

Basement rocks exposed in Zanskar can be divided into three lithotectonic groups: (1) the Tethyan Sedimentary Sequence, or Tethyan Himalaya; (2) the High Himalayan Crystalline Sequence, or Greater Himalaya; and (3) the Indus Suture Zone (Fig. 3). Exposures of these groups are structurally controlled by orogen parallel structures related to SW-verging thrust

nappes and the Zanskar Shear Zone (ZSZ)(Dèzes et al., 1999). The ZSZ represents a ~150 km long strand of the South Tibetan Detachment (Herren, 1987), the major tectonic boundary that separates the Greater and Tethyan Himalaya in this part of the orogen (Burchfiel et al., 1992; Burchfiel and Royden, 1985).

The Tethyan Himalaya is a package of Neoproterozoic to early Paleocene sandstones, limestones, dolostones, and shales classically considered to have been deposited as a passive margin sequence on the northern margin of Greater India (Gaetani et al., 1986; Gaetani et al., 1983; Garzanti et al., 1986; Green et al., 2008). Tethyan Himalayan rocks are very low- to low-grade metasedimentary rocks, although parallel to the ZSZ and Nyimaling-Tso Morari gneiss dome Neoproterozoic-Ordovician formations locally reach lower amphibolite facies (e.g., Dèzes et al., 1999; Fuchs, 1987; Gaetani et al., 1986; Steck, 1993).

Paleozoic magmatism produced two igneous suites observed in the Zanskar region: (1) Pan-African Cambro-Ordovician granitic plutons and (2) Mississippian-Permian granitic plutons associated with Panjal Traps flood basalts. U-Pb zircon ages constrain Pan-African (or Bhimphedian) Orogeny plutonism from ~435 to ~483 Ma (Cawood et al., 2007; Girard and Bussy, 1999; Godin, 2001; Horton and Leech, 2013; Noble and Searle, 1995; Pognante et al., 1990). Later Gondwanan rifting produced isolated granitic plutons dating 268–305 Ma (Horton and Leech, 2013; Noble et al., 2001; Spring et al., 1993) as well as Panjal Traps flood basalts at ~289 Ma (Shellnutt et al., 2011; Shellnutt et al., 2014; Singh et al., 1976).

Structurally below the Tethyan Himalaya and forming the core of the High Himalaya in Zanskar are the exhumed high-grade equivalents of the Neoproterozoic-Ordovician Tethyan Himalaya and late Paleozoic granitic intrusions, collectively referred to as the Greater Himalaya (Dèzes et al., 1999; Honegger, 1983; Horton and Leech, 2013; Pognante et al., 1990; Pognante

and Lombardo, 1989; Schlup et al., 2003; Schlup et al., 2011; Searle et al., 1992; Walker et al., 2001). The Greater Himalaya in Zanskar consists of amphibolite to lower granulite facies Neoproterozoic-early Cambrian paragneiss and metapelite (Herren, 1987), Cambro-Ordovician orthogneiss (Frank et al., 1977; Horton et al., 2015; Mehta, 1977; Noble and Searle, 1995; Pognante et al., 1990; Stutz and Thöni, 1987; Walker et al., 1999) and Mississippian-Permian orthogneiss (Honegger et al., 1982; Horton and Leech, 2013; Noble et al., 2001; Spring et al., 1993).

Rapid exhumation of the Greater Himalaya between the Main Central Thrust (MCT) and ZSZ from 26 Ma (Robyr et al., 2006) to ~17 Ma (Leloup et al., 2010) induced partial melting and injection of leucogranitic melts into the Greater and lower Tethyan Himalayan series (Dèzes et al., 1999; Noble and Searle, 1995; Robyr et al., 2006). Exhumation of Greater Himalayan material continued until ~16 Ma in the south of Zanskar to ~8 Ma around the Nyimaling-Tso Morari gneiss dome (Schlup et al., 2003; Schlup et al., 2011). No significant neotectonic activity in the Zanskar region is observed (Jade et al., 2010).

Sedimentation related to the collision of Greater India and Eurasia is documented in the third lithotectonic group, the Indus Suture Zone (e.g., Searle, 1983; Searle et al., 1990). Thrust slices of ophiolitic mélange, Indus Molasse sandstones, and Cretaceous-Eocene forearc basin strata are exposed near the Zanskar-Indus confluence (Clift et al., 2002a; Henderson et al., 2010; Pedersen et al., 2001; Searle et al., 1990).

METHODS

We use several complementary methods to constrain the provenance of modern sediment in the Zanskar River and understand how bulk sediment compositions evolve downstream before

reaching the Indus River confluence. Sediment samples from the Zanskar River and its major tributaries were collected from 2012 to 2014 during monsoon seasons from active channel beds and point bars (Table 1). We preferentially sampled very fine- to medium sand (>63 μm) because this size fraction is commonly targeted for single-grain mineral provenance techniques that often limit evaluation of finer grain sizes owing to analytical spot size. By only targeting the bedload we cannot consider how suspended load contributes to provenance and this introduce biases to our analyses (Garzanti et al., 2011; Garzanti et al., 2009). However, we argue that our selected size fraction can be considered representative of the bulk zircon provenance (Yang et al., 2012) and provide important initial constraints on patterns of erosion in the Zanskar River basin.

Basin Morphology

We evaluated basin-wide and river channel morphology by extracting topographic parameters and longitudinal river profile data from digital elevation models. Topographic parameters were generated from the void-filled Shuttle Radar Topography Mission (SRTM) V4 90-m digital elevation model (Jarvis et al., 2008) provided by the Consultative Group on International Agricultural Research (http://srtm.csi.cgiar.org) and post-processed with an iterative fill routine (Whipple et al., 2007). Slope values were calculated using a 1 km-radius circular moving window. Local relief, expressed as maximum elevation difference, was calculated using a 5 km-radius circular moving window. Mean annual rainfall values were generated from the 1998–2009 Tropical Rainfall Measuring Mission (TRMM) 2B31 and 2B42 data products for the Himalaya (Bookhagen and Burbank, 2010). Extent of modern glaciers in the Zanskar River basin were derived from the Global Land Ice Measurements from Space (GLIMS) Version 1 data (Shrestha et al., 2014).

Longitudinal river profiles were generated from digital elevation model (DEM) and smoothed every 2 km to remove elevation spikes. Under topographic steady-state, local channel slopes (S) follow a simple power-law scaling relationship with upstream drainage area (A):

$$k_s = S/A^{-\theta} \quad (1)$$

where k_s is the channel steepness index and θ is the concavity index (Flint, 1974; Hack, 1957). Channel steepness is often dependent on uplift rate but other pertinent factors, such as rock strength, precipitation, sediment flux, channel width, and channel hydraulic geometry, commonly influence this relationship (e.g., Craddock et al., 2007; Lavé and Avouac, 2001; Roe et al., 2002; Sklar and Dietrich, 1998; Tucker and Whipple, 2002; Whipple and Tucker, 2002). Discrimination of abrupt breaks in channel steepness can help identify factors perturbing model channel morphologies Application of this index to longitudinal river profiles has become a powerful quantitative tool for extracting information about the relationship between regional tectonics, topography and erosion in fluvial systems (e.g., DiBiase et al., 2010; Kirby and Whipple, 2001; Whipple and Tucker, 2002).

In this study we applied a fixed reference concavity, $\theta_{ref,} = 0.45$, to facilitate comparison of data between river basins (Wobus et al., 2006) and generate a normalized channel steepness index, k_{sn}. Following a methodology similar to Ouimet et al. (2009), we used the freely available MatLab and ArcMap scripts (http://www.geomorphtools.org) to generate k_{sn} values every 2 km for all major tributaries draining >100 km^2.

Bulk Sediment Petrography

Bulk, unsieved sediments were counted in thin section with at least 200 points following the Gazzi-Dickinson method (Ingersoll et al., 1984) with lithic fragments classified after

Garzanti and Vezzoli (2003) by noting the composition and metamorphic rank of rock fragments (MI Index). Thin sections were stained with alizarin red-S to distinguish calcite from dolomite. Sands were classified according to the relative proportion of quartz, feldspar, and lithic material in each sample exceeding 10%.

Hydrodynamic processes can produce significant variability in the composition of sediments with identical provenance (Frihy et al., 1995; Garzanti et al., 2009; Gazzi et al., 1973). We can correct for this environmental bias and limit intrasample variability by applying a "Source Rock Density" (SRD) correction to our petrographic data (Garzanti and Andò, 2007a; Vermeesch et al., 2016). The relative abundance of mineral phases are adjusted according to their densities for each sample and corrected to a suitable SRD value appropriate for provenance type and erosion level (Garzanti and Andò, 2007a, b).We corrected our data using a SRD of 2.71 g/cm^3. Bulk petrographic data are reported in Table 2.

Major and Trace Element Geochemistry

Samples were analyzed for major and trace elements to provide a base characterization of the composition and the degree of chemical alteration. Carbonate was not removed prior to total digestion. All samples were freeze-dried and ground before mixing 600 mg of sample with 3600 mg of lithium tetraborate (LiB_4O_7; Spectromelt). Samples were pre-oxidized at 500°C with NH_4NO_3 and fused to glass beads. Samples were analyzed by X-Ray Fluorescence for Si, Al, Ti, Fe, Na, Ca, K, P and Rb using a Philips PW 2400 X-ray spectrometer at the Institut für Chemie und Biologie des Meeres (ICBM) at the Carl von Ossietzky Universität, Oldenburg, Germany. Measurements on the XRF were followed after Böning et al. (2009). To assure accuracy and

precision, several in-house standards and the certified standard of GSD-12 were analyzed, and results were better than 3%. Data are presented in Table 3.

Isotope Geochemistry

All sediments were analyzed for Sr and Nd isotopes as these isotopic systems can provide complementary insight on chemical weathering and provenance in sedimentary systems. Sr isotopic compositions are largely a function of the age and composition of silicate bedrock but chemical weathering is known to elevate $^{87}Sr/^{86}Sr$ values (Derry and France-Lanord, 1996). However, when provenance can be constrained by a system unaffected by transport or diagenetic processes, such as the largely immobile Sm-Nd system (Goldstein et al., 1984), the paired Rb-Sr and Sm-Nd isotopic systems make a powerful provenance proxy for siliciclastic sediments that has a proven track record in the NW Himalaya (e.g.,Clift et al., 2002b). The bulk silicate sediment fraction was analyzed for most samples, but a few samples only allowed analysis of the <300 μm fraction.

Samples were first leached using buffered acetic acid to remove any carbonate-bound Sr prior to total digestion. Mn-Fe oxides containing authigenic Sr, and potentially any material bearing authigenic Nd, were removed with a leach of 25% (v/v) acetic acid and 0.02 M hydroxylamine hydrochloride (HH). All Sr and Nd signatures measured are therefore assumed to originate from the silicate fraction, perhaps with minor fractions of dolomite. Leached sediments were digested in closed PTFE-vessels following the procedure described in Böning et al. (2004). Briefly, organic matter was oxidized from all samples by treatment with concentrated HNO_3 overnight. Subsequently, HF and $HClO_4$ were added and the vessels were heated for 12 h at 180°C. After digestion, solutions were evaporated on a heated metal block (180°C) and residues

were redissolved, fumed three times with 6N HCl, and dissolved finally in 1N HNO_3. All acids were of ultrapure quality.

To isolate rare earth elements (REEs) and Sr, the remaining solutions were put through two-step column chemistry using Eichrom TRU-Spec resin. Nd was separated from interfering REEs using Eichrom LN-Spec resin with 0.23–0.25 N HCl as eluant. The fraction containing Rb and Sr was loaded on Eichrom Sr-Spec columns using HNO_3, Rb was washed out with HNO_3, and Sr was eluted with Milli-Q water.

Isotopic compositions of Nd and Sr were analyzed using a Thermo Neptune Plus Multicollector ICP-MS at the ICBM in Oldenburg. Samples for Nd were analyzed using the Nd standard JNdi-1. The $^{143}Nd/^{144}Nd$ values of all samples were corrected for internal mass fractionation using $^{146}Nd/^{144}Nd = 0.7219$ and normalized to the reported JNdi-1 value of $^{143}Nd/^{144}Nd = 0.51215$ (Tanaka et al., 2000). Internal mass fractionation for Nd was corrected for using $^{146}Nd/^{144}Nd = 0.7219$. Nd isotopic compositions are expressed in ε_{Nd} notation:

$$\varepsilon_{Nd} = [(^{143}Nd/^{144}Nd)_{sample} / (^{143}Nd/^{144}Nd)_{CHUR} - 1] * 10^4 \quad (2)$$

$(^{143}Nd/^{144}Nd)_{CHUR}$ is the Chondritic Uniform Reservoir with a value of 0.512638 (Jacobsen and Wasserburg, 1980). The external reproducibility is calculated for each session separately using the analyses of JNdi-1 and was generally better than ±0.000015 or ± 0.3 ε_{Nd} units (2σ). The BCR-2 standard (n = 4) had an ε_{Nd} value of 0.1 (± 0.3, 2σ) and was well within the reported ε_{Nd} value of 0.0 ± 0.2 (Raczek et al., 2003). The procedural blank was ≤ 30 pg Nd.

Samples for Sr were analyzed using standard-sample bracketing techniques using NBS987 and normalized to the reported value of 0.710248 (Thirlwall, 1991). Mass fractionation for Sr was corrected using $^{86}Sr/^{88}Sr = 0.1194$. Contents of Kr, Rb, and Ba were monitored and found to be negligible. The external reproducibility is calculated using the analyses of NBS987

and was generally better than 80 ppm (2σ). The BCR-2 standard (n = 4) had a $^{87}Sr/^{86}Sr$ ratio of 0.70502 ± 0.00004 (2σ) and was within the reported $^{87}Sr/^{86}Sr$ ratio of 0.70496 ± 0.00002 (Raczek et al., 2003). The procedural blanks were negligible throughout. Results are reported in Table 4.

Detrital Zircon U-Pb Geochronology

Detrital zircon U-Pb dating has an established history of resolving questions on sediment provenance within Himalayan river systems (e.g., Alizai et al., 2011; Amidon et al., 2005) and in other drainage basins in Asia (e.g., He et al., 2013; Robinson et al., 2014). Zircon is a common mineral and is chemically and mechanically resistant to erosion, such that several cycles of erosion and sedimentation do not significantly alter U and Pb compositions (Gehrels, 2014). In this study we target the 63–250 μm size fraction because this range can effectively yield the same distribution of all significant age populations present in the bulk zircon population (Yang et al., 2012).

The use of U-Pb zircon dating for the Zanskar River is especially appropriate because there are a significant number of existing U-Pb zircon bedrock analyses from Himalaya bedrock. Although lithostratigraphic units in the western Himalaya have zircon populations that overlap, strong preferential occurrence of certain age groups can aid in identifying regions of sediment yield. (e.g., Bernet et al., 2006; Clift et al., 2004; DeCelles et al., 2004; Gehrels et al., 2011; Hu et al., 2015; Shellnutt et al., 2014; White et al., 2011; Wu et al., 2007).

Samples were separated for zircon using standard magnetic and heavy liquid separation techniques. A rare-earth element hand magnet was passed several times over the sample to remove extremely magnetic material and sieved again to 63–250 μm before magnetic separation. All samples were pre-treated using hydrogen peroxide, acetic acid, and oxalic acid to remove

organic material, carbonate, and Fe-oxides, respectively. Zircons were mounted in epoxy, polished, and imaged by reflected light and cathodoluminescence.

U-Th-Pb isotopic compositions were determined at the London Geochronology Centre facilities at University College London using a New Wave 193 nm aperture-imaged frequency-quintupled laser ablation system, coupled to an Agilent 7700 quadrupole-based ICP–MS. An energy density of ~2.5 J/cm^2 and a repetition rate of 10 Hz were used during laser operation. Laser spot diameter was ~30 μm with sampling depth of ~5 μm. Sample-standard bracketing by measurement of external zircon standard PLESOVIC (Sláma et al., 2008) and NIST 612 silicate glass (Pearce et al., 1997) were used to correct for instrumental mass bias and depth-dependent intra-element fractionation of Pb, Th and U. Temora (Black et al., 2003) and 91500 (Wiedenbeck et al., 2004) were used as secondary zircon age standards. Over 100 grains were analyzed for each sample to provide a statistically robust dataset for lithologically diverse units (Vermeesch, 2004). Age data were filtered using a ± 15% discordance cut-off. For grains with ages less than 1000 Ma, the $^{206}Pb/^{238}U$ ratio was used and the $^{207}Pb/^{206}Pb$ ratio for grains older than 1000 Ma. All measurements were processed using GLITTER 4.4 data reduction software (Griffin et al., 2008). Sample-standard bracketing by measurement of external zircon standard PLESOVIC (Sláma et al., 2008) and NIST 612 silicate glass (Pearce et al., 1997) were used to correct for instrumental mass bias and depth-dependent intra-element fractionation of Pb, Th and U. Temora (Black et al., 2003) and 91500 (Wiedenbeck et al., 2004) were used as secondary zircon age standards. Over 100 grains were analyzed for each sample to provide a statistically robust dataset for lithologically diverse units (Vermeesch, 2004). Age data were filtered using a ± 15% discordance cut-off. For grains with ages less than 1000 Ma, the $^{206}Pb/^{238}U$ ratio was used and the $^{207}Pb/^{206}Pb$ ratio for grains older than 1000 Ma. All measurements were processed using

GLITTER 4.4 data reduction software (Griffin et al., 2008). Time-resolved signals recording isotopic ratios with depth in each crystal enabled filtering to remove signatures owing to overgrowth boundaries, inclusions and/or fractures. Individual U-Pb ages are reported at 1σ.

Kernel density estimations (KDE) provide robust age distributions and are presented in the text for visual analysis of age population distributions and abundance. Traditional probability density functions may smooth older age populations that inherently have a greater age error than younger populations at 1σ, therefore KDEs are favored in this study to prevent this bias (Vermeesch, 2012). Multidimensional scaling (MDS) was performed using R.info Version 3.1.1 programming codes modified after Vermeesch (2013) to quantitatively compare zircon spectra.

RESULTS

Basin Morphology

A large-scale rainfall gradient exists across Zanskar from the southwest to the northeast (Fig. 2, 4A), with highest mean annual rainfall (>650 $mm \cdot yr^{-1}$) values observed in the northwest inside the Stod River catchment. Lowest values (<150 $mm \cdot yr^{-1}$) occur around Tso Kar (Fig. 1C). Steepest slopes are in the Stod and Khurna catchments, as well as the Zanskar Gorge, (Fig. 4B), that correspondingly also indicate regions of highest local relief (Fig. 4C).

Zanskar channel profile geometries (Figure 5) indicate strong glacial modification. Remnants of multiple recessional moraines exist in the lower Tsarap River, the overdeepened Stod and Khurna Rivers, and the steep, headwater Tsarap tributaries. The broad, alluviated Padum Basin ends with a terminal moraine at Hanumil (Fig. 1C). The Zanskar Gorge can be characterized in general as a large knickzone. Reworking of a recessional moraine results in a

small knickzone in the lower Tsarap River, although the knickzone is likely enhanced in part by a remaining artifact in the DEM data.

Normalized channel steepness values (Fig. 4D) correspond to several locations for recessional moraines in small, headwater tributaries, and in the lower Tsarap, Khurna and Markha Rivers (Fig. 5). The highest k_{sn} values (>500) occur in the upper Zanskar Gorge and in short segments in the middle reaches of the Tsarap River containing bedrock gorges. We do not include k_{sn} values for the presently endorheic Tso Kar basin (Fig. 4D) but do include other morphometric parameters for this region for reference.

Bulk Sediment Petrography

The Zanskar River transports an incredible diversity of sands that range from lithic carbonaticlastic to feldspatho-quartzolithic metamorphiclastic compositions (Table 2). Framework petrography indicates abundant quartz, feldspar, low rank metacarbonate, high-rank fibrolite-bearing metafelsite fragments, with minor chert, epidote-bearing metabasite, and serpentinized ultramafic rock fragments. Abundant mineral grains include calcite and dolomite spar, mica, sillimanite, green amphibole, and ultrastable minerals such as zircon, blue-green tourmaline, rutile, and titanite. Minor kyanite, garnet, staurolite, and brown amphibole are noted. Most sands contain moderate amounts of mica and/or dense minerals but most carbonaticlastic sands are poor in both micaceous and dense phases.

Zanskar River sediments roughly divide into two petrographic groups (Fig. 6). Samples containing slightly more lithic fragments, predominantly more carbonate and lesser volcanic fragments, fall within rocks of Tethyan Himalayan affinity (Fig. 6A). Samples that are slightly more quartzofeldspathic lie closer to rocks with Greater Himalayan affinity. Similarly, samples

with higher grade metamorphic minerals fall nearer rocks of known Greater Himalayan affinity (Fig. 6B).

Major and Trace Element Geochemistry

Major element geochemistry can be effective in assessing the intensity of chemical weathering. The "Chemical Index of Alteration" proxy expressed as:

$CIA = ((Al_2O_3/(Al_2O_3+Na_2O+K_2O+CaO^*)) \bullet 100$ (3)

can be used to compare the relative leaching of labile elements (K, Na, silicate-only Ca) to residual, immobile Al during feldspar weathering (Nesbitt et al., 1980). CIA values range from 50 to 100 with higher values indicating stronger chemical weathering. A correction is made to CIA values if excess CaO is present in carbonates and phosphates by assuming a reasonable Ca/Na ratio for the silicate material and correcting for CaO in phosphate (Singh et al., 2005).

Zanskar River sediments (Table 3; Fig. 7) span low to moderate CIA values (52–71). In general, higher CIA values occur in upstream tributaries and lower values, indicating less intense weathering, occur in the lower Tsarap (ID #9) and Stod (ID #7, #8) Rivers, and Padum Basin sediment samples of Pishu (#5) and Hanumil (ID #4). CIA values are poorly correlated to SiO_2, with slight negative correlation as silica contents increase.

Isotope Geochemistry

Variations in Sr and Nd isotopes for Zanskar River sediments and regional bedrock source terranes are plotted in Figure 8. Isotopic compositions for decarbonated Zanskar River sediments display a range in ε_{Nd} values from -10 to -17.4 and a wide range of $^{87}Sr/^{86}Sr$ isotope values from 0.713990 to 0.755070. No coherent correlation exists between the isotopic systems.

The widest variation in $^{87}Sr/^{86}Sr$ values occurs in the upstream Tsarap River tributaries (Fig. 9). The Zara (ID #10), lower Tsarap (ID #9), and Yunam (ID #13) River samples display the greatest enrichment, and Gata (ID #12) one of the least enriched. The Stod River (ID #7, #8) sediments remain remarkably consistent with a $^{87}Sr/^{86}Sr$ value of ~0.723. After the confluence with the Stod River, $^{87}Sr/^{86}Sr$ values become only slightly less enriched down the Zanskar River as the Oma (ID #3) and Markha (ID #2) Rivers join the trunk river.

The Stod River, in contrast to the Sr isotopes, demonstrates a shift to more negative ε_{Nd} values downstream (Fig. 9). Similar ε_{Nd} values are seen at Yunam (ID #13) and Gata (ID #11), as well as at Toze Lungpa (ID #11) and Zara (ID #10). Curiously, the trunk sample at Pishu (ID #5) demonstrates a more negative ε_{Nd} value than either the lower Stod (ID #7) or Tsarap (ID# 9) Rivers after they join. Downstream of Pishu (ID #5), the trunk river values do not vary significantly even downstream of the more positive Markha (ID #2) and Oma (ID #3) River confluences.

Detrital U-Pb Zircon Geochronology

All dated Zanskar River samples are presented as kernel density estimate (KDE) diagrams following Vermeesch (2004) in Figure 10. All Zanskar age analyses are presented in Table S1. Most samples contain one or more peak populations at 245–380 Ma, 440–500 Ma, 500–600 Ma, and 750–850 Ma. Some samples have a composite peak from 750–1250 Ma comprised of smaller subsidiary peaks at ~900 Ma, ~1000 Ma and ~1100 Ma. Paleoproterozoic and Archean peaks are found from 1600–1900 Ma and at ~2500 Ma, with very few ages at ~3200 Ma and ~3400 Ma.

Lower Stod (ID #7), Pishu (ID #5), Hanumil (ID #4), and Zanskar-Indus (ID #1) confluence samples display similar age spectra to one another, with very prominent peaks at 750–850 Ma, and with two smaller peaks at ~350 Ma and ~450 Ma. Tsarap tributary samples populate a second group that also display the prominent ~450 Ma Ma peak but contain older ages clustered at ~530 Ma, the broad 750–1250 Ma peak and an older, less populous peak from 1600–1900 Ma. The Zara (ID #10), Lower Tsarap (ID #9), Markha (ID #2), and to a lesser extent Yunam (ID #13), samples contain small peaks at ~2500 Ma.

Zircons less than 300 Ma were uncommon in most samples but some tributaries yielded Mesozoic and Cenozoic ages. Pishu (ID #5), Hanumil (ID#4) and the Zanskar-Indus confluence (ID #1) yield zircon with ages clustered at ~260 Ma. Toze Lungpa (ID #11) was the only sample that yielded five zircon with a latest Triassic-earliest Jurassic mean age of 209 ± 6 Ma. The Markha River yielded two late Cretaceous ages, one at 130.5 ± 3.4 Ma and 97.2 ± 2.8 Ma. One late Paleocene age at 57.7 ± 1.1 Ma was yielded from the Zanskar-Indus confluence. Three samples (Lower Stod, Hanumil, Pishu) contained Oligocene and Miocene grains with ages ranging from 18–32 Ma.

DISCUSSION

Downstream provenance evolution

Little variability in Sr and Nd isotopic compositions is observed in the trunk river downstream of Padum. The Zanskar-Indus (ID #1) confluence sample is most comparable to the Lower Stod River (ID #7; Fig. 9). Even so, Sr values decrease and Nd values increase slightly downstream of Padum suggesting minor addition of sediment from smaller (<100 km2) Zanskar Gorge tributaries (Fig. 5). This sediment must be isotopically similar to the Oma (ID#3) and

Markha (ID#2) Rivers because of the observed decrease in $^{87}Sr/^{86}Sr$ values and increase in ε_{Nd}. Nonetheless, contribution from the Oma River is negligible as the trunk river does not change its ε_{Nd} value downstream of this confluence.

Much of the geochemical variability in Zanskar River sediments occurs upstream of Padum before the confluence of the Lower Stod (ID #7) and Tsarap (ID #9) Rivers. $^{87}Sr/^{86}Sr$ values from the Upper (ID #8) and Lower Stod are within error of each other, but the Upper Stod is marked by a more positive ε_{Nd} value. The downstream decrease in ε_{Nd} values along the Stod River likely results from contribution of felsic, less radiogenic crystalline Greater Himalaya (ε_{Nd} = -15.2 ± 2.2; (Robinson et al., 2001). Sediment from Panjal Traps basalts (ε_{Nd} = -8–0; (Shellnutt et al., 2014) added into the Upper Stod can account for the more positive ε_{Nd} values seen.

The Tsarap River drains almost all lithologies exposed in the Zanskar River basin and this in part rationalizes the wide variability observed in Tsarap catchment isotope compositions (Lower Tsarap (ID# 9), Toze Lungpa (ID #11), Zara (ID #10), Yunam (ID #13)). We conclude that the Lower Tsarap sample is not representative of a Tsarap catchment-averaged composition. This is because the ε_{Nd} value observed at Pishu (ID #5; ε_{Nd} = -15.5) after mixing of the Lower Stod (ID #7; ε_{Nd} = -14.5) requires that the net contribution from the Tsarap be more negative than -15.5 (consistent with measurements in the upper Tsarap), in contrast to the measured Lower Tsarap sample (ID #9; ε_{Nd} = -13.6). This raises the possibility that the Lower Tsarap sample is locally derived. Alternatively, this sample could represent a transient pulse of sediment in the Tsarap derived from enhanced erosion sourced from similar bedrock and/or sediments further upstream, perhaps linked to older, large volume mass movements triggered by climatic events (e.g., cloud bursts, (Hobley et al., 2012)).

Bulk petrography and detrital zircon analyses suggest two models for sediment mixing downstream (Fig. 11). Framework grains indicate a continued, progressive compositional evolution of sediments downstream, with marginally greater contribution of sediment from the Stod River (ID #7, #8) than other tributaries. In contrast, detrital zircon grains demonstrate an overwhelming dominance of material sourced from the Stod River and little variation in zircon populations downstream of Padum. MDS analysis of detrital zircon samples clearly segregates sediments into two groups, whereas bulk petrography and major element compositions form slightly less discrete groups (Figs. 12A-C). Selected source bedrock U-Pb age data are plotted for comparison in Figures 12D and S1.

Below the Tsarap (ID #9) and Stod (ID #7) River confluence at Padum, each detrital zircon sample on the trunk river contains 600–850 Ma grains as the majority population (Fig. 11). A small increase in >2400 Ma ages at the Zanskar-Indus (ID #1) confluence, however, does suggest minor contribution from the Markha River (ID #2). Bulk petrography also argues for an additional contribution from the Markha and Oma (ID#3) Rivers, and likely other small Zanskar Gorge tributaries. After exiting the gorge in the lower reaches, river sediments contain more Tethyan sedimentary and low-grade metasedimentary lithics than below Hanumil (ID #4) at the gorge entrance.

Lithic grains of trunk river samples above the gorge display closest similarity to the Lower Tsarap (ID #9) River (Figs. 11 and 12). Pishu (ID #5, #6) and Hanumil (ID# 4) samples contain abundant Tethyan Himalayan metapelitic and carbonate fragments, with very few high-grade, coarsely crystalline Greater Himalayan gneiss and calc-gneiss fragments. Although these trunk river samples do not contain a lot of high-grade lithic fragments, the abundance of quartz, feldspar and fibrolite still indicate strong contribution of Greater Himalayan material. This

sediment is likely sourced in part from the Cambro-Ordovician and Mississippian-Permian granitic gneisses exposed as part of the Greater Himalaya along the ZSZ, rather than from the Zara River (Fig. 3). The abundance of quartzofeldspathic, micaceous, and schistose metamorphiclastic detritus in the Zara (ID #10) sample might suggest an overspill connection existed between Tso Kar and the Zanskar River, as proposed by Demske et al. (2009) and Wünnemann et al. (2010). Our provenance data from the Zara River neither support nor preclude sediment supply to the Zanskar River via an overspill connection (e.g,, Munack et al., 2016). Potential parent bedrock sources to the Zara River are exposed immediately northeast, outside the Tso Kar basin, as well as along strike into that basin and further southeast to Tso Morari. Furthermore, we suggest the Zara River does not contribute much Nyimaling-Tso Morari gneiss dome material to trunk river samples because none is found in bulk sediments lower in the Tsarap River (Fig. 11). Similarly, the Yunam River (ID #13) carries abundant Greater Himalayan metamorphic material but is simply diluted by the Tethyan Himalayan sedimentary fragments sourced from other tributaries downstream.

Detrital zircon populations with central ages at ~350 Ma, ~450 Ma, and ~530 Ma (Fig. 10) support previous findings for abundant Cambro-Ordovician and Mississippian-Permian granites found in the Greater Himalaya in Zanskar and elsewhere in the northwest Himalaya (Fig. S2; Honegger et al., 1982; Horton and Leech, 2013; Spring et al., 1993). Detrital zircon ages clustered at ~260 Ma could be sourced from Panjal Traps but are younger than the reported ages (~289 Ma) northeast of Zanskar (Shellnutt et al., 2014; Singh et al., 1976). Permian granites are not recognized in Greater Himalaya units from the eastern and central Himalaya (Gehrels et al., 2011). The relative lack or presence of such prominent age peaks between the central/eastern

and northwest Himalaya encourages future caution when using detrital zircon compilations to correlate strata across the orogen when such heterogeneities exists (Fig. S2).

Heavy mineral fertility likely plays a role in the apparent contrast observed between bulk petrography and detrital zircon analyses. For example, detrital zircon ages at Yunam (ID #13) appear to be transmitted downstream to Gata (ID #11; Figs. 9 and 11), consistent with a stable ε_{Nd} value over that stretch of river. However, the bulk petrography and Sr isotope values change markedly between these two samples, requiring significant sediment dilution. This discrepancy requires that either the material being added has the same zircon and Nd-bearing phases but different bulk lithologic composition, or that the sediment contributed from tributaries between Yunam and Gata (ID #11) is lacking in those phases. We favor the latter as being more likely.

Controls on Erosion

While our dataset cannot quantify sediment yields, we here provide the first initial constraints on sediment provenance and the relative contributions of sources downstream in the Zanskar River. The data presented above yield a clear image of the Stod River being a significant source of sediment to the Zanskar. This influence is moderated by downstream sediment contributions from tributaries and minor, side valley tributaries. We argue that the bulk of sediment production in the Zanskar River is driven by strong glacial erosion in the Stod River valley and lesser hillslope erosion across the catchment. We favor glacial erosion as the primary process controlling erosion because westernmost Zanskar and Stod River hillslopes and valleys have been strongly modified by glaciation for at least the last 78 k.y. (Taylor and Mitchell, 2000) and continue to be conditioned by active alpine glaciers. Glaciers comprise ~28% of the modern Stod River basin versus 7-8% of the modern Tsarap and overall Zanskar River basins. Spatial

patterns of erosion in Zanskar may not correlate significantly with convexities in river profiles caused by lithologic changes or high channel steepness (Figs. 2 and 5). Instead, the highest yields come from the Stod River catchment that contains a broad, overdeepened and alluviated U-shaped valley, steep hillslopes housing north-facing glaciers, low to moderate k_{sn} values, and convexities along the river profile that reflect earlier glacial conditioning.

Hillslope processes acting at high elevation in semi-arid regions cannot be ruled out as significant producers of sediment. Soil creep, grussification, granulation, and salt weathering are known to generate sediment along the Indus River valley but are likely less influential than (peri-) glacial and fluvial processes in driving bedrock erosion and evacuating sediment in paraglacial environments (Blöthe et al., 2015; Dietsch et al., 2015; Hales and Roering, 2007; Scherler, 2014). Hillslope processes operate at slower rates and the material that is produced is not readily mobilized. Erosion in drier, unglaciated catchments in Zanskar is likely strongly driven by slow hillslope processes but unlikely operating at comparable rates or volumes as glaciated catchments.

Bookhagen et al. (2005a) indicate that mass wasting is fundamental in driving increased sediment flux and shaping landscapes in the dry Himalayan interior. Debris flows and deep-seated landslides are facilitated when intense summer rainfall destabilizes poorly vegetated hillslopes. Over the Holocene, mass wasting events correlate well with periods of enhanced monsoonal rainfall in steep rain shadow reaches (Bookhagen et al., 2005b; Dortch et al., 2009). Our findings do not support rainfall-modulated landsliding as a primary control on modern erosion in the Zanskar River. The few mass wasting deposits identified in the basin neither correlate with modern erosion patterns nor major knickzones.

Seasonal summer monsoonal precipitation, however, may provide a first-order control on sediment transport. We propose that glacial erosion drives production of unconsolidated sediments that are then later reworked during high-intensity monsoon events in the modern Zanskar River basin. Snow and glacial meltwater cause heightened discharge and suspended sediment flux in the dry Himalaya during the early summer (Anderson et al., 2004; Burbank et al., 2012), but later monsoonal storm events more effectively drive sediment transport. The magnitude of glacial sediment production and/or flux of reworked sediment from the Stod River catchment is great enough that significant dilution of this signal does not occur downstream, even after addition of mobilized hillslope sediments. This is in contrast to what has been observed in the frontal Himalaya where glacial sediment production is masked by much stronger monsoonal erosion (Godard et al., 2012). Erosion in Zanskar also contrasts to that seen in the unglaciated basins along the Indus valley that receive <115 $mm \bullet yr^{-1}$ precipitation and have extremely slow integrated rates of erosion (Dietsch et al., 2015; Dortch et al., 2011b; Munack et al., 2014). We argue that sediment production and transport in the Zanskar River basin are modulated by the same primary drivers of erosion (i.e., glaciers and monsoon rainfall), but that these operate at different relative magnitudes compared to the frontal Himalaya, as well as the more slowly denuding regions along the Indus Valley.

Our study of modern erosion patterns in the Zanskar River naturally solicits comparisons between contemporary and Quaternary erosive conditions. While modern sediments in semi-arid to arid Ladakh and Zanskar may in part be mobilized during high intensity storm events (e.g., Hobley et al., 2012; Stolle et al., 2015), it cannot be assumed that these conditions held true in the past. Stronger Holocene monsoon phases at 8–10 ka and 30–35 ka brought enhanced precipitation onto Tibetan Plateau margins that promoted greater vegetative cover (Demske et

al., 2009; Herzschuh, 2006; Shi et al., 2001; Wünnemann et al., 2010). Increased slope stability as a result of more vegetation could reduce the erosive capability of high-intensity storm perturbations and potentially reduce erosional response (e.g., Beaumont et al., 2000). Under prolonged enhanced monsoonal conditions, it is unlikely storm events had equivalent impacts over the region, and if these events had similar recurrence, transience, and magnitude. In light of the devastating debris flows in 2010 and 2015 in Ladakh, more work is needed to understand the nature of these high intensity events and their erosional impact.

Next, our work begs the question whether the material yielded from the Stod River is eroded from bedrock or primarily reworked from glacial moraines. We cannot definitively untangle the relative contribution of reworked glacial material at least with our dataset, however, based on the present observation of abundant incised glaciofluvial terraces we prefer the idea that large-scale recycling of material generated during the Last Glacial Maximum is the primary source of sediment to the Stod River. Furthermore we recognize that longer term glacial and monsoonal phases dictating sediment generation and reworking might be disrupted by shorter duration, perhaps stochastic, climatic perturbations. However, the generally cohesive trends in our provenance data would indicate that the modern signal is not dominated by these events.

Significant dissection of Pleistocene valley-fills in the upper Tsarap catchment highlights a long history of sediment reworking into the paleo-Zanskar River (Munack et al., 2016). Although our data here do not indicate a strong contemporary contribution from these deposits to the modern Zanskar River, to what extent the provenance signal may have been distorted as a result of such recycling in the past remains open to investigation. This combined understanding of erosion in Zanskar further emphasizes that sediment buffering over millennial to even multi-

millennial timescales is likely an important process controlling sediment routing in the Himalayan rain shadow and the overall transfer of climate-erosion signals downstream.

CONCLUSIONS

We applied a suite of geochemical and geochronological techniques to establish spatial patterns of erosion in a rain shadow river system. Our findings demonstrate that modern sediment provenance in Zanskar is driven by focused glacial erosion and monsoonal rainfall along the Greater Himalaya and Zanskar Shear Zone. The Stod River catchment, representing only 13% of the total area of the Zanskar River basin, dominates in delivering sediment to the modern drainage. The distribution of erosion in Zanskar is not directly controlled by monsoonal rainfall as is the case in the frontal Himalaya, but rather the precipitation gradient promotes a concentration of permanent, north-facing glaciers that efficiently scour the High Himalaya. The Zanskar differs from its wetter neighbors to the south in being less controlled by mass wasting but also differs from drier, formerly glaciated catchments further north in having enough precipitation to regularly mobilize the sediment produced by glaciation. Dry, low relief, unglaciated regions of Zanskar contribute minimally to the total modern sediment flux. We suggest that increased flux from these arid regions may only be significant when extreme monsoon storms, or even prolonged, intense Holocene monsoon phases, mobilize sediments from unvegetated hillslopes.

Our data are broadly consistent with the glacially-dominated sediment production model of Blothe et al. (2014), but here our analyses the potential importance of monsoon precipitation in remobilizing sediment and allowing its transportation into the main Indus River system. While the majority of sediment may be fluxed during deglacial and post-glacial times, we argue that it

monsoon may control sediment transport rather than deglaciation itself (c.f., Blöthe et al., 2014). This appears to be true at least in the present day in this transitional setting between the wet frontal Himalaya and the arid orogenic interior of the Tibetan Plateau. In the absence of tectonic forcing in Zanskar, our results support climatic control on erosion in the Himalaya. If surface processes dominate over million year timescales then these would shape orogenic architecture in the way favored by critical wedge and channel flow extrusion models (Beaumont et al., 2001; Robinson et al., 2006).

ACKNOWLEDGMENTS

This work was supported by the Charles T. McCord Jr. Chair in petroleum geology at LSU and in part by the Farouk El-Baz Student Research Award, and LSU scholarships. This manuscript was greatly improved by thoughtful and constructive reviews by Jason Dortch and Jan Blöthe. TJ and PC thank Fida Hussein Mittoo with Rockland Tourism and Arundeep Aluwahlia from Panjab University for logistical support. TJ would like to thank Eduardo Garzanti for valuable discussions on sediment petrography and Jan Blöthe and Henry Munack on Zanskar geomorphology. PB and KP thank the ICBM and Max Planck Institute for Marine Microbiology for financial support.

REFERENCES CITED

Alizai, A., Carter, A., Clift, P. D., VanLaningham, S., Williams, J. C., and Kumar, R., 2011, Sediment provenance, reworking and transport processes in the Indus River by U–Pb dating of detrital zircon grains: Global and Planetary Change, v. 76, no. 1-2, p. 33–55, doi:10.1016/j.gloplacha.2010.11.008.

Amidon, W. H., Burbank, D. W., and Gehrels, G. E., 2005, U-Pb zircon ages as a sediment mixing tracer in the Nepal Himalaya: Earth and Planetary Science Letters, v. 235, no. 1-2, p. 244–260, doi:10.1016/j.epsl.2005.03.019.

Anderson, J. L., and Bender, E. E., 1989, Nature and origin of Proterozoic A-type granitic magmatism in the southwestern United States of America: Lithos, v. 23, no. 1, p. 19–52, doi:10.1016/0024-4937(89)90021-2.

Anderson, R. S., Anderson, S. P., MacGregor, K. R., Waddington, E. D., O'Neel, S., Riihimaki, C. A., and Loso, M. G., 2004, Strong feedbacks between hydrology and sliding of a small alpine glacier: Journal of Geophysical Research: Earth Surface, v. 109, no. F3, p. F03005, doi: 10.1029/2004JF000120.

Attal, M., and Lavé, J., 2006, Changes of bedload characteristics along the Marsyandi River (central Nepal): Implications for understanding hillslope sediment supply, sediment load evolution along fluvial networks, and denudation in active orogenic belts: Geological Society of America Special Papers, v. 398, p. 143-171, doi: 10.1130/2006.2398(09).

Beaumont, C., Jamieson, R. A., Nguyen, M. H., and Lee, B., 2001, Himalayan tectonics explained by extrusion of a low-viscosity crustal channel coupled to focused surface denudation: Nature, v. 414, no. 6865, p. 738–742, doi:10.1038/414738a.

Beaumont, C., Kooi, H., and Willett, S., 2000, Coupled tectonic-surface process models with applications to rifted margins and collisional orogens: Geomorphology and global tectonics, p. 29-55,

Bernet, M., van der Beek, P., Pik, R., Huyghe, P., Mugnier, J.-L., Labrin, E., and Szulc, A. G., 2006, Miocene to Recent exhumation of the central Himalaya determined from combined detrital zircon fission-track and U/Pb analysis of Siwalik sediments, western Nepal: Basin Research, v. 18, p. 393–412, 10.1111/j.1365-2117.2006.00303.x.

Black, L. P., Kamo, S. L., Allen, C. M., Aleinikoff, J. N., Davis, D. W., Korsch, R. J., and Foudoulis, C., 2003, TEMORA 1: a new zircon standard for Phanerozoic U-Pb geochronology: Chemical Geology, v. 200, p. 155–170, doi:10.1016/S0009-2541(03)00165-7.

Blöthe, J. H., Korup, O., and Schwanghart, W., 2015, Large landslides lie low: Excess topography in the Himalaya-Karakoram ranges: Geology, v. 43, no. 6, p. 523-526,

Blöthe, J. H., Munack, H., Korup, O., Fülling, A., Garzanti, E., Resentini, A., and Kubik, P. W., 2014, Late Quaternary valley infill and dissection in the Indus River, western Tibetan Plateau margin: Quaternary Science Reviews, v. 94, p. 102–119, doi:10.1016/j.quascirev.2014.04.011.

Böning, P., Brumsack, H.-J., Schnetger, B., and Grunwald, M., 2009, Trace metal signatures of Chilean upwelling sediments at ~36°S: Marine Geology, v. 259, p. 112–121, doi:10.1016/j.margeo.2009.01.004.

Bookhagen, B., 2010, Appearance of extreme monsoonal rainfall events and their impact on erosion in the Himalaya: Geomatics, Natural Hazards and Risk, v. 1, no. 1, p. 37–50, doi: 10.1080/19475701003625737.

Bookhagen, B., and Burbank, D. W., 2006, Topography, relief, and TRMM-derived rainfall variations along the Himalaya: Geophysical Research Letters, v. 33, no. L08405, p. L08405 doi: 10.1029/2006GL026037.

Bookhagen, B., and Burbank, D. W., 2010, Towards a complete Himalayan hydrological budget: The spatiotemporal distribution of snow melt and rainfall and their impact on river discharge: Journal of Geophysical Research Earth Surface (2003–2012), v. 115, p. F03019, doi: 10.1029/2009JF001426.

Bookhagen, B., Thiede, R. C., and Strecker, M. R., 2005a, Abnormal monsoon years and their control on erosion and sediment flux in the high, arid northwest Himalaya: Earth and Planetary Science Letters, v. 231, no. 1-2, p. 131–146, doi: 10.1016/j.epsl.2004.11.014.

Bookhagen, B., Thiede, R. C., and Strecker, M. R., 2005b, Late Quaternary intensified monsoon phases control landscape evolution in the northwest Himalaya: Geology, v. 33, no. 2, p. 149–152, doi: 10.1130/G20982.1.

Burbank, D., and Fort, M., 1985, Bedrock control on glacial limits: examples from the Ladakh and Zanskar ranges: north-western Himalaya, India: Journal of Glaciology, v. 31, no. 108, p. 143–149,

Burbank, D. W., Blythe, A. E., Putkonen, J., Pratt-Sitaula, B., Gabet, E. J., Oskin, M., Barros, A., and Ojha, T., 2003, Decoupling of erosion and precipitation in the Himalayas: Nature, v. 426, p. 652–655, doi: 10.1038/nature02187.

Burbank, D. W., Bookhagen, B., Gabet, E. J., and Putkonen, J., 2012, Modern climate and erosion in the Himalaya: Comptes Rendus Geoscience, v. 344, no. 11-12, p. 610–626, doi: 10.1016/j.crte.2012.10.010.

Burchfiel, B. C., Chen, Z., Hodges, K. V., Liu, Y., Royden, L. H., Deng, C., and Xu, J., 1992, The South Tibetan Detachment System, Himalayan Orogen: Extension Contemporaneous With and Parallel to Shortening in a Collisional Mountain Belt, Special Paper - Geological Society of America, Volume 269: Boulder, CO, Geological Society of America, p. 1–41, doi: 10.1130/SPE269-p1.

Burchfiel, B. C., and Royden, L., 1985, North-south extension within the convergent Himalayan region: Geology, v. 13, no. 10, p. 679–682, doi: 10.1130/0091-7613(1985) 13<679:NEWTCH>2.0.CO;2

Cawood, P. A., Johnson, M. R., and Nemchin, A. A., 2007, Early Palaeozoic orogenesis along the Indian margin of Gondwana: tectonic response to Gondwana assembly: Earth and Planetary Science Letters, v. 255, no. 1–2, p. 70–84, doi:10.1016/j.epsl.2006.12.006.

Clift, P. D., Campbell, I. H., Pringle, M. S., Carter, A., Zhang, X., Hodges, K. V., Khan, A. A., and Allen, C. M., 2004, Thermochronology of the modern Indus River bedload: New insight into the controls on the marine stratigraphic record: Tectonics, v. 23, no. 5, p. TC5013, doi: 10.1029/2003TC00155.

Clift, P. D., Carter, A., and Jonell, T. N., 2014, U–Pb dating of detrital zircon grains in the Paleocene Stumpata Formation, Tethyan Himalaya, Zanskar, India: Journal of Asian Earth Sciences, v. 82, p. 80–89, doi: 10.1016/j.jseaes.2013.12.014.

Clift, P. D., Carter, A., Krol, M., and Kirby, E., 2002a, Constraints on India-Eurasia collision in the Arabian Sea region taken from the Indus Group, Ladakh Himalaya, India, *in* Clift, P. D., Kroon, D., Gaedicke, C., and Craig, J., eds., The tectonic and climatic evolution of the Arabian Sea region, Volume 195: London, Geological Society, p. 97–116, doi: 10.1144/GSL.SP.2002.195.01.07.

Clift, P. D., Hodges, K. V., Heslop, D., Hannigan, R., Van Long, H., and Calves, G., 2008, Correlation of Himalayan exhumation rates and Asian monsoon intensity: Nature Geoscience, v. 1, no. 12, p. 875–880, doi: 10.1038/ngeo351.

Clift, P. D., Lee, J. I., Hildebrand, P., Shimizu, N., Layne, G. D., Blusztajn, J., Blum, J. D., Garzanti, E., and Khan, A. A., 2002b, Nd and Pb isotope variability in the Indus River system; implications for sediment provenance and crustal heterogeneity in the western Himalaya: Earth and Planetary Science Letters, v. 200, no. 1-2, p. 91–106, doi: 10.1016/S0012-821X(02)00620-9.

Clift, P. D., Shimizu, N., Layne, G. D., Blusztajn, J. S., Gaedicke, C., Schlüter, H. U., Clark, M. K., and Amjad, S., 2001, Development of the Indus Fan and its significance for the erosional history of the Western Himalaya and Karakoram: Geological Society of America Bulletin, v. 113, no. 8, p. 1039–1051, doi: 10.1130/0016-7606(2001)113<1039:DOTIFA>2.0.CO;2.

Condie, K. C., 1993, Chemical composition and evolution of the upper continental crust: contrasting results from surface samples and shales: Chemical geology, v. 104, no. 1–4, p. 1–37, doi: 10.1016/0009-2541(93)90140-E.

Craddock, W. H., Burbank, D. W., Bookhagen, B., and Gabet, E. J., 2007, Bedrock channel geometry along an orographic rainfall gradient in the upper Marsyandi River valley in central Nepal: Journal of Geophysical Research: Earth Surface v. 112, no. F3, p. F03007, doi: 10.1029/2006JF000589.

Damm, B., 2006, Late Quaternary glacier advances in the upper catchment area of the Indus River (Ladakh and western Tibet): Quaternary International, v. 154–155, p. 87–99, doi: 10.1016/j.quaint.2006.02.013.

DeCelles, P. G., Gehrels, G. E., Najman, Y., Martin, A. J., Carter, A., and Garzanti, E., 2004, Detrital geochronology and geochemistry of Cretaceous-Early Miocene strata of Nepal: implications for timing and diachroneity of initial Himalayan orogenesis: Earth and Planetary Science Letters, v. 227, no. 3–4, p. 313–330, doi: 10.1016/j.epsl.2004.08.019.

DeCelles, P. G., Gehrels, G. E., Quade, J., LaReau, B., and Spurlin, M., 2000, Tectonic implications of U-Pb zircon ages of the Himalayan orogenic belt in Nepal: Science, v. 288, no. 5465, p. 497–499, doi: 10.1126/science.288.5465.497.

Demske, D., Tarasov, P. E., Wünnemann, B., and Riedel, F., 2009, Late glacial and Holocene vegetation, Indian monsoon and westerly circulation in the Trans-Himalaya recorded in the lacustrine pollen sequence from Tso Kar, Ladakh, NW India: Palaeogeography, Palaeoclimatology, Palaeoecology, v. 279, no. 3-4, p. 172-185, 10.1016/j.palaeo.2009.05.008.

Derry, L. A., and France-Lanord, C., 1996, Neogene Himalayan weathering history and river $^{87}Sr/^{86}Sr$; impact on the marine Sr record: Earth and Planetary Science Letters, v. 142, no. 1–2, p. 59–74, doi: 10.1016/0012-821X(96)00091-X.

Dèzes, P. J., Vannay, J. C., Steck, A., Bussy, F., and Cosca, M., 1999, Synorogenic extension: quantitative constraints on the age and displacement of the Zanskar shear zone (Northwest Himalaya): Geological Society of America Bulletin, v. 111, no. 3, p. 364–374, doi: 10.1130/0016-7606(1999)111<0364:SEQCOT>2.3.CO;2.

DiBiase, R. A., Whipple, K. X., Heimsath, A. M., and Ouimet, W. B., 2010, Landscape form and millennial erosion rates in the San Gabriel Mountains, CA: Earth and Planetary Science Letters, v. 289, no. 1–2, p. 134–144, doi: 10.1016/j.epsl.2009.10.036.

Dietsch, C., Dortch, J. M., Reynhout, S. A., Owen, L. A., and Caffee, M. W., 2015, Very slow erosion rates and landscape preservation across the southwestern slope of the Ladakh Range, India: Earth Surface Processes and Landforms, v. 40, no. 3, p. 389–402, doi: 10.1002/esp.3640.

Dortch, J. M., Dietsch, C., Owen, L. A., Caffee, M. W., and Ruppert, K., 2011a, Episodic fluvial incision of rivers and rock uplift in the Himalaya and Transhimalaya: Journal of the Geological Society, v. 168, no. 3, p. 783–804, doi: 10.1144/0016-76492009-158.

Dortch, J. M., Owen, L. A., and Caffee, M. W., 2013, Timing and climatic drivers for glaciation across semi-arid western Himalayan–Tibetan orogen: Quaternary Science Reviews, v. 78, p. 188–208, doi: 10.1016/j.quascirev.2013.07.025.

Dortch, J. M., Owen, L. A., Haneberg, W. C., Caffee, M. W., Dietsch, C., and Kamp, D. U., 2009, Nature and timing of large-landslides in the Himalaya and Transhimalaya of northern India: Quaternary Science Reviews, v. 28, no. 11–12, p. 1037–1054, doi: 10.1016/j.quascirev.2008.05.002.

Dortch, J. M., Owen, L. A., Schoenbohm, L. M., and Caffee, M. W., 2011b, Asymmetrical erosion and morphological development of the central Ladakh Range, northern India: Geomorphology, v. 135, no. 1-2, p. 167-180, 10.1016/j.geomorph.2011.08.014.

Fedo, C. M., Nesbitt, H. W., and Young, G. M., 1995, Unraveling the effects of potassium metasomatism in sedimentary rocks and paleosols, with implications for paleoweathering conditions and provenance: Geology, v. 23, no. 10, p. 921–924, doi: 10.1130/0091-7613(1995)023<0921:UTEOPM>2.3.CO;2.

Flint, J. J., 1974, Stream gradient as a function of order, magnitude, and discharge: Water Resources Research, v. 10, no. 5, p. 969–973, doi: 10.1029/WR010i005p00969.

Frank, W., Thöni, M., and Purtscheller, F., Geology and petrography of Kulu-South Lahul area, *in* Proceedings Colloq. Internat. CNRS Himalaya1977, Volume 268, p. 147–160,

Frihy, O., Lotfy, M., and Komar, P., 1995, Spatial variations in heavy minerals and patterns of sediment sorting along the Nile Delta, Egypt: Sedimentary Geology, v. 97, no. 1, p. 33–41, doi: 10.1016/0037-0738(94)00135-H.

Fuchs, G., 1987, The Geology of Southern Zanskar (Ladakh) - Evidence for the Autochthony of the Tethys Zone of the Himalaya: Jahrbuch der Geologischen Bundesanstalt, v. 130, no. 4, p. 465–491,

Gabet, E. J., Burbank, D. W., Pratt-Sitaula, B., Putkonen, J., and Bookhagen, B., 2008, Modern erosion rates in the High Himalayas of Nepal: Earth and Planetary Science Letters, v. 267, no. 3, p. 482–494, doi: 10.1016/j.epsl.2007.11.059.

Gaetani, M., Casnedi, P., Fois, E., Garzanti, E., Jadoul, F., Nicora, A., and Tintori, A., 1986, Stratigraphy of the Tethys Himalaya in Zanskar, Ladakh: Rivista Italiana di Paleontologia e Stratigrafia, v. 91, no. 4, p. 443–478,

Gaetani, M., Nicora, A., Silva, I. P., Fois, E., Garzanti, E., and Tintori, A., 1983, Upper Cretaceous and Paleocene in Zanskar Range (NW Himalaya), Istituti di geologia e paleontologia dell'Università degli studi di Milano, Riv. It. Paleont. Strat.,

Garzanti, E., and Andò, S., 2007a, Heavy mineral concentration in modern sands: implications for provenance interpretation, *in* Mange, M. A., and Wright, D. T., eds., Heavy Minerals in Use, Volume 58, Elsevier, p. 517–545, doi: 10.1016/S0070-4571(07)58020-9.

-, 2007b, Plate tectonics and heavy mineral suites of modern sands, *in* Mange, M. A., and Wright, D. T., eds., Heavy Minerals in Use, Volume 58, Elsevier, p. 741–763, doi: 10.1016/S0070-4571(07)58029-5.

Garzanti, E., Andó, S., France-Lanord, C., Censi, P., Vignola, P., Galy, V., and Lupker, M., 2011, Mineralogical and chemical variability of fluvial sediments 2. Suspended-load silt (Ganga–Brahmaputra, Bangladesh): Earth and Planetary Science Letters, v. 302, no. 1–2, p. 107–120, doi: 10.1016/j.epsl.2010.11.043.

Garzanti, E., Andò, S., and Vezzoli, G., 2009, Grain-size dependence of sediment composition and environmental bias in provenance studies: Earth and Planetary Science Letters, v. 277, no. 3–4, p. 422–432, doi: 10.1016/j.epsl.2008.11.007.

Garzanti, E., Casnedi, R., and Jadoul, F., 1986, Sedimentary evidence of a Cambro-Ordovician orogenic event in the northwestern Himalaya: Sedimentary Geology, v. 48, no. 3–4, p. 237–265, doi: 10.1016/0037-0738(86)90032-1.

Garzanti, E., and Vezzoli, G., 2003, A classification of metamorphic grains in sands based on their composition and grade: Journal of Sedimentary Research, v. 73, no. 5, p. 830–837, DOI: 10.1306/012203730830.

Garzanti, E., Vezzoli, G., Andò, S., Lavé, J. r. m., Attal, M. l., France-Lanord, C., and DeCelles, P., 2007, Quantifying sand provenance and erosion (Marsyandi River, Nepal Himalaya): Earth and Planetary Science Letters, v. 258, no. 3–4, p. 500–515, doi: 10.1016/j.epsl.2007.04.010.

Gazzi, P., Zuffa, G. G., Gandolfi, G., and Paganelli, L., 1973, Provenienza e dispersione litoranea delle sabbie delle spiagge adriatiche fra le foci dell'Isonzo e del Foglia: inquadramento regionale: Memorie della Società Geologica Italiana, v. 12, p. 1–37,

Gehrels, G. E., 2014, Detrital zircon U-Pb geochronology applied to tectonics: Annual Review of Earth and Planetary Sciences, v. 42, p. 127–149, doi: 10.1146/annurev-earth-050212-124012.

Gehrels, G. E., Kapp, P., DeCelles, P., Pullen, A., Blakely, R., Weislgel, A., Ding, L., Guynn, J., Marin, A., McQuarrie, N., and Yin, A., 2011, Detrital zircon geochronology of pre-Tertiary strata in the Tibetan-Himalayan orogen: Tectonics, v. 30, no. 5, p. TC5016, doi 10.1029/2011TC002868.

Girard, M., and Bussy, F., 1999, Late Pan-African magmatism in the Himalaya: new geochronological and geochemical data from the Ordovician Tso Morari metagranites (Ladakh, NW India): Schweizerische mineralogische und petrographische Mitteilungen, v. 79, no. 3, p. 399–418,

Godard, V., Burbank, D. W., Bourlès, D. L., Bookhagen, B., Braucher, R., and Fisher, G. B., 2012, Impact of glacial erosion on ^{10}Be concentrations in fluvial sediments of the Marsyandi catchment, central Nepal: Journal of Geophysical Research: Earth Surface, v. 117, no. F3, p. F03013, doi: 10.1029/2011JF002230.

Godin, L., 2001, The Chako Dome: an enigmatic structure in the hanging wall of the South Tibetan detachment, Nar Valley central Nepal: Journal of Asian Earth Sciences, v. 19, no. 3A, p. 22–23,

Goldstein, S. L., O'Nions, R. K., and Hamilton, P. J., 1984, A Sm-Nd isotopic study of atmospheric dusts and particulates from major river systems: Earth and Planetary Science Letters, v. 70, no. 2, p. 221–236, doi: 10.1016/0012-821X(84)90007-4.

Goodbred, S. L., 2003, Response of the Ganges dispersal system to climate change: a source-to-sink view since the last interstade: Sedimentary Geology, v. 162, no. 1–2, p. 83–104, doi: 10.1016/S0037-0738(03)00217-3.

Green, O. R., Searle, M. P., Corfield, R. I., and Corfield, R. M., 2008, Cretaceous-Tertiary carbonate platform evolution and the age of the India-Asia collision along the Ladakh

Himalaya (northwest India): The Journal of Geology, v. 116, no. 4, p. 331–353, doi: 10.1086/588831.
Griffin, W. L., Powell, W. J., Pearson, N. J., and O'Reilly, S. Y., 2008, GLITTER: data reduction software for laser ablation ICP-MS: Laser Ablation-ICP-MS in the earth sciences. Mineralogical association of Canada short course series, v. 40, p. 204–207,
Hack, J. T., 1957, Studies of longitudinal stream profiles in Virginia and Maryland, 2330-7102,
Hales, T., and Roering, J. J., 2007, Climatic controls on frost cracking and implications for the evolution of bedrock landscapes: Journal of Geophysical Research: Earth Surface, v. 112, no. F2,
He, M., Zheng, H., and Clift, P. D., 2013, Zircon U–Pb geochronology and Hf isotope data from the Yangtze River sands: Implications for major magmatic events and crustal evolution in Central China: Chemical Geology, v. 360–261, p. 186–203, doi: 10.1016/j.chemgeo.2013.10.020.
Hedrick, K. A., Seong, Y. B., Owen, L. A., Caffee, M. W., and Dietsch, C., 2011, Towards defining the transition in style and timing of Quaternary glaciation between the monsoon-influenced Greater Himalaya and the semi-arid Transhimalaya of Northern India: Quaternary International, v. 236, no. 1–2, p. 21–33, doi: 10.1016/j.quaint.2010.07.023.
Henderson, A. L., Najman, Y., Parrish, R., BouDagher-Fadel, M., Barford, D., Garzanti, E., and Andò, S., 2010, Geology of the Cenozoic Indus Basin sedimentary rocks: Paleoenvironmental interpretation of sedimentation from the western Himalaya during the early phases of India-Eurasia collision Tectonics, v. 29, no. 6, p. TC6015, doi: 10.1029/2009TC002651.
Herren, E., 1987, Zanskar Shear Zone: northeast-south- west extension within the Higher Himalaya: Geology, v. 15, no. 5, p. 409–413, doi: 10.1130/0091-7613(1987) 15<409:ZSZNEW>2.0.CO;2.
Herzschuh, U., 2006, Palaeo-moisture evolution in monsoonal Central Asia during the last 50,000 years: Quaternary Science Reviews, v. 25, no. 1-2, p. 163-178, 10.1016/j.quascirev.2005.02.006.
Hobley, D. E., Sinclair, H. D., and Mudd, S. M., 2012, Reconstruction of a major storm event from its geomorphic signature: The Ladakh floods, 6 August 2010: Geology, v. 40, no. 6, p. 483–486, doi: 10.1130/G32935.1.
Hodges, K. V., Wobus, C., Ruhl, K., Schildgen, T., and Whipple, K., 2004, Quaternary deformation, river steepening, and heavy precipitation at the front of the Higher Himalayan ranges: Earth and Planetary Science Letters, v. 220, no. 3–4, p. 379–389, doi: 10.1016/S0012-821X(04)00063-9.
Honegger, K., Dietrich, V., Frank, W., Gansser, A., Thoni, M., and Trommsdorf, V. F., 1982, Magmatism and metamorphism in the Ladakh Himalayas (The Indus-Tsangpo suture zone): Earth and Planetary Science Letters, v. 60, no. 2, p. 253–292, doi: 10.1016/0012-821X(82)90007-3.
Honegger, K. H., 1983, Strukturen und metamorphose im ZanskarkristallinPhD]: Eidgenössiche Technische Hochschule (E.T.H.), 117 p,
Horton, F., Lee, J., Hacker, B., Bowman-Kamaha'o, M., and Cosca, M., 2015, Himalayan gneiss dome formation in the middle crust and exhumation by normal faulting: New geochronology of Gianbul dome, northwestern India: Geological Society of America Bulletin, v. 127, no. 1–2, p. 162–180, doi: 10.1130/B31005.1.

Horton, F., and Leech, M. L., 2013, Age and origin of granites in the Karakoram shear zone and Greater Himalaya Sequence, NW India: Lithosphere, v. 5, no. 3, p. 300–320, doi: 10.1130/L213.1.

Hu, X.-M., Garzanti, E., An, W., and Hu, X.-F., 2015, Provenance and drainage system of the Early Cretaceous volcanic detritus in the Himalaya as constrained by detrital zircon geochronology: Journal of Palaeogeography, v. 4, no. 1, p. 85–98, doi: 10.3724/SP.J.1261.2015.00069.

Hu, X.-M., Sinclair, H. D., Wang, J., Jiang, H., and Wu, F., 2012, Late Cretaceous-Palaeogene stratigraphic and basin evolution in the Zhepure Mountain of southern Tibet: implications for the timing of India-Asia initial collision: Basin Research, v. 24, no. 5, p. 520–543, doi: 10.1111/j.1365-2117.2012.00543.x.

Ingersoll, R. V., Bullard, T. F., Ford, R. L., Grimm, J. P., Pickle, J. D., and Sares, S. W., 1984, The effect of grain size on detrital modes: A test of the Gazzi-Dickinson point-counting method: Journal of Sedimentary Petrology, v. 54, no. 1, p. 103–116, doi: 10.1306/212F83B9-2B24-11D7-8648000102C1865D.

Jacobsen, S. B., and Wasserburg, G. J., 1980, Sm-Nd isotopic evolution of chondrites: Earth and Planetary Science Letters, v. 50, no. 1, p. 139–155, doi: 10.1016/0012-821X(80)90125-9.

Jade, S., Rao, H. J. R., Vijayan, M. S. M., Gaur, V. K., Bhatt, B. C., Kumar, K., Jaganathan, S., Ananda, M. B., and Kumar, P. D., 2010, GPS-derived deformation rates in northwestern Himalaya and Ladakh: International Journal of Earth Sciences, v. 100, no. 6, p. 1293–1301, doi: 10.1007/s00531-010-0532-3.

Jarvis, A., Reuter, H. I., Nelson, A., and Guevara, E., 2008, Hole-filled SRTM for the globe Version 4, *in* Research, C. G. o. I. A., ed., CGIAR-CSI SRTM 90m Database http://srtm.csi.cgiar.org,

Kirby, E., and Ouimet, W., 2011, Tectonic geomorphology along the eastern margin of Tibet: Insights into the pattern and processes of active deformation adjacent to the Sichuan Basin, *in* Gloaguen, R., and Ratschbacher, L., eds., Growth and Collapse of the Tibetan Plateau, Volume 353: London, Geological Society, p. 165–188, doi: 10.1144/SP353.9.

Kirby, E., and Whipple, K., 2001, Quantifying differential rock-uplift rates via stream profile analysis: Geology, v. 29, no. 5, p. 415–418, doi: 10.1130/0091-7613(2001)029<0415:QDRURV>2.0.CO;2.

Kwatra, S. K., Singh, S., Singh, V. P., Sharma, R. K., Rai, B., and Kishor, N., 1999, Geochemical and geochronological characteristics of the Early Paleozoic granitoids from Sutlej-Baspa Valleys, Himachal Himalayas: Gondwana Research Group Memoirs, v. 6, p. 145–158,

Lavé, J., and Avouac, J. P., 2001, Fluvial incision and tectonic uplift across the Himalaya of central Nepal: Journal of Geophysical Research, v. 106, no. B11, p. 26561–26592, doi: 10.1029/2001JB000359.

Leipe, C., Demske, D., Tarasov, P. E., Wünnemann, B., and Riedel, F., 2014, Potential of pollen and non-pollen palynomorph records from Tso Moriri (Trans-Himalaya, NW India) for reconstructing Holocene limnology and human–environmental interactions: Quaternary International, v. 348, p. 113–129, doi: 10.1016/j.quaint.2014.02.026.

Leloup, P. H., Mahéo, G., Arnaud, N., Kali, E., Boutonnet, E., Liu, D., Xiaohan, L., and Haibing, L., 2010, The South Tibet detachment shear zone in the Dinggye area Time constraints on extrusion models of the Himalayas: Earth and Planetary Science Letters, v. 292, no. 1–2, p. 1–16, doi:10.1016/j.epsl.2009.12.035.

McQuarrie, N., Robinson, D., Long, S., Tobgay, T., Grujic, D., Gehrels, G., and Ducea, M., 2008, Preliminary stratigraphic and structural architecture of Bhutan: Implications for the along strike architecture of the Himalayan system: Earth and Planetary Science Letters, v. 272, no. 1–2, p. 105–117, doi: 10.1016/j.epsl.2008.04.030.

Mehta, P. K., 1977, Rb-Sr geochronology of the Kulu-Mandi belt: its implications for the Himalayan tectogenesis: Geologische Rundschau, v. 66, no. 1, p. 156–175, doi: 10.1007/BF01989570.

Miller, C., Thöni, M., Frank, W., Grasemann, B., Klötzli, U., Guntli, P., and Draganits, E., 2001, The early Palaeozoic magmatic event in the Northwest Himalaya, India: source, tectonic setting and age of emplacement: Geological Magazine, v. 138, no. 03, p. 237–251, doi: 10.1017/S0016756801005283.

Milliman, J. D., and Meade, R. H., 1983, World-wide delivery of sediment to the oceans: Journal of Geology, v. 91, no. 1, p. 1–21,

Mitchell, W. A., Taylor, P. J., and Osmaston, H., 1999, Quaternary geology in Zanskar, NW Indian Himalaya: evidence for restricted glaciation and preglacial topography: Journal of Asian Earth Sciences, v. 17, no. 3, p. 307–318, doi: 10.1016/S0743-9547(98)00069-5.

Munack, H., Blöthe, J. H., Fülöp, R. H., Codilean, A. T., Fink, D., and Korup, O., 2016, Recycling of Pleistocene valley fills dominates 135 ka of sediment flux, upper Indus River: Quaternary Science Reviews, v. 149, p. 122-134, http://dx.doi.org/10.1016/j.quascirev.2016.07.030.

Munack, H., Korup, O., Resentini, A., Limonta, M., Garzanti, E., Blöthe, J. H., Scherler, D., Wittmann, H., and Kubik, P. W., 2014, Postglacial denudation of western Tibetan Plateau margin outpaced by long-term exhumation: Geological Society of America Bulletin, v. 126, no. 11–12, p. 1580–1594, doi: 10.1130/B30979.1.

Myrow, P. M., Hughes, N. C., Goodge, J. W., Fanning, C. M., Williams, I. S., Peng, S., Bhargava, O. N., Parcha, S. K., and Pogue, K. R., 2010, Extraordinary transport and mixing of sediment across Himalayan central Gondwana during the Cambrian-Ordovician: Geological Society of America Bulletin, v. 122, no. 9–10, p. 1660–1670, doi: 10.1130/B30123.1.

Myrow, P. M., Hughes, N. C., Paulsen, T., Williams, I., Parcha, S. K., Thompson, K. R., Bowring, S. A., Peng, S.-C., and Ahluwalia, A. D., 2003, Integrated tectonostratigraphic analysis of the Himalaya and implications for its tectonic reconstruction: Earth and Planetary Science Letters, v. 212, no. 3–4, p. 433–441, doi: 10.1016/S0012-821X(03)00280-2.

Nesbitt, H. W., Markovics, G., and Price, R. C., 1980, Chemical processes affecting alkalis and alkaline earths during continental weathering: Geochimica et Cosmochimica Acta, v. 44, no. 11, p. 1659–1666, doi: 10.1016/0016-7037(80)90218-5.

Noble, S. R., and Searle, M. P., 1995, Age of Crustal Melting and Leukogranite Formation from U-Pb Zircon and Monazite Dating in the Western Himalaya, Zanskar, India: Geology, v. 23, no. 12, p. 1135–1138, doi: 10.1130/0091-7613(1995)023<1135:AOCMAL>2.3.CO;2.

Noble, S. R., Searle, M. P., and Walker, C. B., 2001, Age and tectonic significance of Permian granites in western Zanskar, High Himalaya: Journal of Geology, v. 109, no. 1, p. 127–135,

Ouimet, W. B., Whipple, K. X., and Granger, D. E., 2009, Beyond threshold hillslopes: Channel adjustment to base-level fall in tectonically active mountain ranges: Geology, v. 37, no. 7, p. 579–582, doi: 10.1130/G30013A.1.

Owen, L. A., 2011, Quaternary Glaciation of Northern India, Developments in Quaternary Science, Volume 15, Elsevier, p. 14, doi: 10.1016/b978-0-444-53447-7.00067-2.
Owen, L. A., and Benn, D. I., 2005, Equilibrium-line altitudes of the last glacial maximum for the Himalaya and Tibet; an assessment and evaluation of results: Quaternary International, v. 138–139, p. 55–78, doi: 10.1016/j.quaint.2005.02.006.
Owen, L. A., Finkel, R. C., Barnard, P. L., Ma, H., Asahi, K., Caffee, M. W., and Derbyshire, E., 2005, Climatic and topographic controls on the style and timing of late Quaternary glaciation throughout Tibet and the Himalaya defined by 10Be cosmogenic radionuclide surface exposure dating: Quaternary Science Reviews, v. 24, no. 12–13, p. 1391–1411, doi: 10.1016/j.quascirev.2004.10.014.
Owen, L. A., Finkel, R. C., and Caffee, M. W., 2002, A note on the extent of glaciation throughout the Himalaya during the global Last Glacial Maximum: Quaternary Science Reviews, v. 21, no. 1–3, p. 147–157, doi: 10.1016/S0277-3791(01)00104-4.
Pearce, N. J. G., Perkins, W. T., Westgate, J. A., Gorton, M. P., Jackson, S. E., Neal, C. R., and Chenery, S. P., 1997, A Compilation of New and Published Major and Trace Element Data for NIST SRM 610 and NIST SRM 612 Glass Reference Materials: Geostandards Newsletter, v. 21, no. 1, p. 115–144, doi: 10.1111/j.1751-908X.1997.tb00538.x.
Pedersen, R. B., Searle, M. P., and Corfield, R. I., 2001, U–Pb zircon ages from the Spontang Ophiolite, Ladakh Himalaya: Journal of the Geological Society, v. 158, no. 3, p. 513–520, doi: 10.1144/jgs.158.3.513.
Pognante, U., Castelli, D., Benna, P., Genovese, G., Oberli, F., Meier, M., and Tonarini, S., 1990, The crystalline units of the High Himalayas in the Lahul-Zanskar region (northwest India): metamorphictectonic history and geochronology of the collided and imbricated Indian plate: Geological Magazine, v. 127, no. 02, p. 101–116, doi: 10.1017/S0016756800013807.
Pognante, U., and Lombardo, B., 1989, Metamorphic evolution of the High Himalayan Crystallines in SE Zanskar, India: Journal of Metamorphic Geology, v. 7, p. 9-17,
Raczek, I., Jochum, K. P., and Hofmann, A. W., 2003, Neodymium and Strontium Isotope Data for USGS Reference Materials BCR-1, BCR-2, BHVO-1, BHVO-2, AGV-1, AGV-2, GSP-1, GSP-2 and Eight MPI-DING Reference Glasses: Geostandards Newsletter, v. 27, no. 2, p. 173–179, doi: 10.1111/j.1751-908X.2003.tb00644.x.
Robinson, D. M., DeCelles, P. G., and Copeland, P., 2006, Tectonic evolution of the Himalayan thrust belt in western Nepal; implications for channel flow models: Geological Society of America Bulletin, v. 118, no. 7-8, p. 865-885,
Robinson, D. M., DeCelles, P. G., Patchett, P. J., and Garzione, C. N., 2001, The kinematic evolution of the Nepalese Himalaya interpreted from Nd isotopes: Earth and Planetary Science Letters, v. 192, no. 4, p. 507–521, doi: 10.1016/S0012-821X(01)00451-4.
Robinson, R. A. J., Brezina, C. A., Parrish, R. R., Horstwood, M. S. A., Oo, N. W., Bird, M. I., Thein, M., Walters, A. S., Oliver, G. J., and Zaw, K., 2014, Large rivers and orogens: The evolution of the Yarlung Tsangpo–Irrawaddy system and the eastern Himalayan syntaxis: Gondwana Research, v. 26, no. 1, p. 112–121, doi: 10.1016/j.gr.2013.07.002.
Robyr, M., Hacker, B. R., and Mattinson, J. M., 2006, Doming in compressional orogenic settings: new geochronological constraints from the NW Himalaya: Tectonics, v. 25, no. 2, p. TC2007, doi: 10.1029/2004TC001774.

Roe, G. H., Montgomery, D. R., and Hallet, B., 2002, Effects of orographic precipitation variations on the concavity of steady-state river profiles: Geology, v. 30, no. 2, p. 143–146, doi: 10.1130/0091-7613(2002)030<0143:EOOPVO>2.0.CO;2.

Scherler, D., 2014, Climatic limits to headwall retreat in the Khumbu Himalaya, eastern Nepal: Geology, v. 42, no. 11, p. 1019-1022,

Schlup, M., Carter, A., Cosca, M., and Steck, A., 2003, Exhumation history of eastern Ladakh revealed by ^{40}Ar-^{39}Ar and fission track ages: The Indus River-Tso Morari transect, NW Himalaya: Journal of the Geological Society, v. 160, p. 385–399, doi: 10.1144/0016-764902-084.

Schlup, M., Steck, A., Carter, A., Cosca, M., Epard, J.-L., and Hunziker, J., 2011, Exhumation history of the NW Indian Himalaya revealed by fission track and ^{40}Ar/^{39}Ar ages: Journal of Asian Earth Sciences, v. 40, no. 1, p. 334–350, doi: 10.1016/j.jseaes.2010.06.008.

Schwanghart, W., and Scherler, D., 2014, Short Communication: TopoToolbox 2 – MATLAB-based software for topographic analysis and modeling in Earth surface sciences: Earth Surf. Dynam., v. 2, no. 1, p. 1-7, 10.5194/esurf-2-1-2014.

Searle, M., Waters, D. J., Rex, D. C., and Wilson, R. N., 1992, Pressure, temperature, and time constraints on Himalayan metamorphism from eastern Kashmir and western Zanskar: Journal of the Geological Society, London, v. 149, p. 753-773,

Searle, M. P., 1983, On the Tectonics of the Western Himalaya: Episodes, no. 4, p. 21-26,

Searle, M. P., Pickering, K. T., and Cooper, D. J. W., 1990, Restoration and Evolution of the Intermontane Indus Molasse Basin, Ladakh Himalaya, India: Tectonophysics, v. 174, no. 3–4, p. 301–314, doi: 10.1016/0040-1951(90)90327-5.

Shellnutt, J., Bhat, G., Brookfield, M., and Jahn, B. M., 2011, No link between the Panjal Traps (Kashmir) and the Late Permian mass extinctions: Geophysical Research Letters, v. 38, no. 19, p. L19308, doi: 10.1029/2011GL049032.

Shellnutt, J. G., Bhat, G. M., Wang, K.-L., Brookfield, M. E., Jahn, B.-M., and Dostal, J., 2014, Petrogenesis of the flood basalts from the Early Permian Panjal Traps, Kashmir, India: Geochemical evidence for shallow melting of the mantle: Lithos, v. 204, p. 159–171, doi: 10.1016/j.lithos.2014.01.008.

Shi, Y., Yu, G., Liu, X., Li, B., and Yao, T., 2001, Reconstruction of the 30–40ka bp enhanced Indian monsoon climate based on geological records from the Tibetan Plateau: Palaeogeography, Palaeoclimatology, Palaeoecology, v. 169, no. 1, p. 69-83, 10.1016/S0031-0182(01)00216-4.

Shrestha, F., Bajracharya, S., Maharjan, S., and Guo, W., 2014, GLIMS Glacier Database Version 1: Boulder, Colorado USA, NSIDC: National Snow and Ice Data Center, http://dx.doi.org/10.7265/N5V98602.

Singh, M., Sharma, M., and Tobschall, H. J., 2005, Weathering of the Ganga alluvial plain, northern India: implications from fluvial geochemistry of the Gomati River: Applied Geochemistry, v. 20, no. 1, p. 1–21, doi: 10.1016/j.apgeochem.2004.07.005.

Singh, M. P., Manda, M. M., and Sinha, P. K., 1976, The Ralakung volcanics of the Zanskar valley (Ladakh), its geological setting, petrography, petrogeochemistry and a comparative study with the Panjal volcanics of the NW Himalaya: Geological Survey of India Miscellaneous Publications, v. 41, p. 218–228,

Sklar, L., and Dietrich, W. E., 1998, River longitudinal profiles and bedrock incision models: Stream power and the influence of sediment supply, *in* Tinkler, K. J., and Wohl, E. E., eds., Rivers over rock: fluvial processes in bedrock channels, Volume Geophysical

Monograph: Washington, D.C., American Geophysical Union, p. 237–260, doi: 10.1029/GM107p0237.
Sláma, J., Košler, J., Condon, D. J., Crowley, J. L., Gerdes, A., Hanchar, J. M., Horstwood, M. S. A., Morris, G. A., Nasdala, L., Norberg, N., Schaltegger, U., Schoene, B., Tubrett, M. N., and Whitehouse, M. J., 2008, Plezovice zircon A new natural reference material for U–Pb and Hf isotopic microanalysis: Chemical Geology, v. 249, no. 1–2, p. 1–35, doi: 10.1016/j.chemgeo.2007.11.005.
Spring, L., Bussy, F., Vannay, J.-C., Huon, S., and Cosca, M., 1993, Early Permian granitic dykes of alkaline affinity in the Indian High Himalaya of Upper Lahul and SE Zanskar: geochemical characterization and geotectonic implications: Geological Society, London, Special Publications, v. 74, no. 1, p. 251–264, doi: 10.1144/GSL.SP.1993.074.01.18.
Srivastava, P., Tripathi, J. K., Islam, R., and Jaiswal, M. K., 2008, Fashion and phases of Late Pleistocene aggradation and incision in Alaknanda River, western Himalaya India: Quaternary Research, v. 70, no. 1, p. 68–80, doi: 10.1016/j.yqres.2008.03.009.
Steck, A., Spring, L., Vannay, J. C., Masson, H., Stutz, E., Bucher, H., ... & Tièche, J. C. , 1993, Geological transect across the northwestern Himalaya in eastern Ladakh and Lahul (a model for the continental collision of India and Asia): Eclogae Geologicae Helvetiae v. 86, no. 1, p. 219–263,
Stolle, A., Langer, M., Blöthe, J. H., and Korup, O., 2015, On predicting debris flows in arid mountain belts: Global and Planetary Change, v. 126, p. 1-13, http://dx.doi.org/10.1016/j.gloplacha.2014.12.005.
Stutz, E., and Thöni, M., 1987, The lower Paleozoic Nyimaling granite in the Indian Himalaya (Ladakh): new Rb/Sr data versus zircon typology: Geologische Rundschau, v. 76, no. 2, p. 307–315, doi: 10.1007/BF01821076.
Tanaka, T., Togashi, S., Kamioka, H., Amakawa, H., Kagami, H., Hamamoto, T., Yuhara, M., Orihashi, Y., Yoneda, S., Shimizu, H., Kunimaru, T., Takahashi, K., Yanagi, T., Nakano, T., Fujimaki, H., Shinjo, R., Asahara, Y., Tanimizu, M., and Dragusanu, C., 2000, JNdi-1: a neodymium isotopic reference in consistency with LaJolla neodymium: Chemical Geology, v. 168, no. 3–4, p. 279–281, doi: 10.1016/S0009-2541(00)00198-4.
Taylor, P. J., and Mitchell, W. A., 2000, The Quaternary glacial history of the Zanskar Range, north-west Indian Himalaya: Quaternary International, v. 65–66, p. 81–99, doi: 10.1016/S1040-6182(99)00038-5.
Thiede, R. C., Bookhagen, B., Arrowsmith, J. R., Sobel, E. R., and Strecker, M. R., 2004, Climatic control on rapid exhumation along the Southern Himalayan Front: Earth and Planetary Science Letters, v. 222, no. 3–4, p. 791–806, doi: 10.1016/j.epsl.2004.03.015.
Thirlwall, M. F., 1991, Long-term reproducibility of multicollector Sr and Nd isotope ratio analysis: Chemical Geology: Isotope Geoscience section, v. 94, no. 2, p. 85–104, doi: 10.1016/0168-9622(91)90002-E.
Tucker, G. E., and Whipple, K. X., 2002, Topographic outcomes predicted by stream erosion models: Sensitivity analysis and intermodel comparison: Journal of Geophysical Research: Solid Earth, v. 107, no. B9, p. ETG 1-1–ETG 1-16, doi: 10.1029/2001JB000162.
Vermeesch, P., 2004, How many grains are needed for a provenance study?: Earth and Planetary Science Letters, v. 224, no. 3–4, p. 351–441, doi: 10.1016/j.epsl.2004.05.037.
Vermeesch, P., 2012, On the visualisation of detrital age distributions: Chemical Geology, v. 312–313, p. 190–194, doi: 10.1016/j.chemgeo.2012.04.021.

Vermeesch, P., 2013, Multi-sample comparison of detrital age distributions: Chemical Geology, v. 341, p. 140–146, doi: 10.1016/j.chemgeo.2013.01.010.
Vermeesch, P., Resentini, A., and Garzanti, E., 2016, An R package for statistical provenance analysis: Sedimentary Geology, v. 336, p. 14–25, doi: 10.1016/j.sedgeo.2016.01.009.
Walker, C. B., Searle, M. P., and Waters, D. J., 2001, An integrated tectonothermal model for the evolution of the High Himalaya in western Zanskar with constraints from thermobarometry and metamorphic modeling: Tectonics, v. 20, no. 6, p. 810–833, doi: 10.1029/2000TC001249.
Walker, J., Martin, M. W., Bowring, S. A., Searle, M., Waters, D. J., and Hodges, K., 1999, Metamorphism, melting, and extension: Age constraints from the High Himalayan Slab of southeast Zanskar and northwest Lahaul: Journal of Geology, v. 107, no. 4, p. 473–495,
Wallis, D., Carter, A., Phillips, R. J., Parsons, A. J., and Searle, M. P., 2016, Spatial variation in exhumation rates across Ladakh and the Karakoram: New apatite fission track data from the Eastern Karakoram, NW India: Tectonics, v. 35, no. 3, p. 704–721, doi: 10.1002/2015TC003943.
Whipple, K., Wobus, C., Crosby, B., Kirby, E., and Sheehan, D., 2007, New tools for quantitative geomorphology: extraction and interpretation of stream profiles from digital topographic data, Geological Society of America Short Course, Volume 506: Boulder, CO, GSA,
Whipple, K. X., and Tucker, G. E., 2002, Implications of sediment-flux-dependent river incision models for landscape evolution: Journal of Geophysical Research: Solid Earth, v. 107, no. B2, p. ETG 3-1-ETG 3-20, 10.1029/2000JB000044.
White, L. T., Ahmad, T., Ireland, T. R., Lister, G. S., and Forster, M. A., 2011, Deconvolving episodic age spectra from zircons of the Ladakh Batholith, northwest Indian Himalaya: Chemical Geology, v. 289, no. 3–4, p. 179–196, doi: 10.1016/j.chemgeo.2011.07.024.
Wiedenbeck, M., Hanchar, J. M., Peck, W. H., Sylvester, P., Valley, J., Whitehouse, M., Kronz, A., Morishita, Y., Nasdala, L., Fiebig, J., Franchi, I., Girard, J. P., Greenwood, R. C., Hinton, R., Kita, N., Mason, P. R. D., Norman, M., Ogasawara, M., Piccoli, P. M., Rhede, D., Satoh, H., Schulz-Dobrick, B., Skår, O., Spicuzza, M. J., Terada, K., Tindle, A., Togashi, S., Vennemann, T., Xie, Q., and Zheng, Y. F., 2004, Further Characterisation of the 91500 Zircon Crystal: Geostandards and Geoanalytical Research, v. 28, no. 1, p. 9–39, doi: 10.1111/j.1751-908X.2004.tb01041.x.
Winter, J. D., 2010, Principles of igneous and metamorphic petrology, New York, Prentice Hall
Wobus, C., Whipple, K. X., Kirby, E., Snyder, N., Johnson, J., Spyropolou, K., Crosby, B., and Sheehan, D., 2006, Tectonics from topography: Procedures, promise, and pitfalls, *in* Willett, S. D., Hovius, N., Brandon, M. T., and Fisher, D. M., eds., Tectonics, Climate, and Landscape Evolution, Volume 398: Boulder, CO, Geological Society of America, p. 55-74, 10.1130/2006.2398(04).
Wu, F. Y., Clift, P. D., and Yang, J. H., 2007, Zircon Hf isotopic constraints on the sources of the Indus Molasse, Ladakh Himalaya, India: Tectonics, v. 26, no. 2, p. TC2014, doi: 10.1029/2006TC002051.
Wulf, H., Bookhagen, B., and Scherler, D., 2010, Seasonal precipitation gradients and their impact on fluvial sediment flux in the Northwest Himalaya: Geomorphology, v. 118, no. 1–2, p. 13-21, doi: 10.1016/j.geomorph.2009.12.003.

Wulf, H., Bookhagen, B., and Scherler, D., 2012, Climatic and geologic controls on suspended sediment flux in the Sutlej River Valley, western Himalaya: Hydrology and Earth System Sciences Discussions, v. 9, p. 541–594, doi: 10.5194/hessd-9-541-2012.

Wünnemann, B., Demske, D., Tarasov, P., Kotlia, B. S., Reinhardt, C., Bloemendal, J., Diekmann, B., Hartmann, K., Krois, J., and Riedel, F., 2010, Hydrological evolution during the last 15kyr in the Tso Kar lake basin (Ladakh, India), derived from geomorphological, sedimentological and palynological records: Quaternary Science Reviews, v. 29, no. 9-10, p. 1138-1155, 10.1016/j.quascirev.2010.02.017.

Yang, S., Zhang, F., and Wang, Z., 2012, Grain size distribution and age population of detrital zircons from the Changjiang (Yangtze) River system, China: Chemical Geology, v. 296-297, p. 26–38, doi: 10.1016/j.chemgeo.2011.12.016.

FIGURE CAPTIONS

Figure 1. Digital elevation model (DEM) maps of South Asia, the Himalaya, and Zanskar River basin. (A) Shuttle Radar Topography Mission 90 m (SRTM90) map of South Asia depicting the Indus River (gray lines) and all Himalayan river drainage outlines above 500 m (black lines). Gray overlay shows location of Figure 4; (B) SRTM DEM and hillshade of all Himalayan drainage basins with location of the Zanskar River basin (Fig. 1C) outlined in black; (C) Topographic map of the Zanskar River basin with sample numbers and locations. Glacial extent from Global Land Ice Measurements from Space (GLIMS) Version 1 data (Shrestha et al., 2014). Drainage basin polygons provided freely online by Bodo Bookhagen. Sample locations noted with white dots and village locations with black squares. Numbers in circles are after Table 1. Dashed gray line indicates extent of internally drained Tso Kar basin.Village names abbreviated as: C = Chilling; HN = Hanumil; PG = Pang; PM = Padum; PS = Pishu; and SR = Sarchu.

Figure 2. Swath profiles for topography and rainfall across the Himalayan front and into the Himalayan rain shadow. Values for profiles were extracted from a 50 km by 280 km transect shown in Fig. 1A. Solid lines indicate mean values with shaded regions signifying ± 2σ.

Figure 3. Simplified geologic map of the Zanskar River basin after Fuchs (1987) with additions from Zanskar Shear Zone from Dèzes et al. (1999), southern Zanskar (Lahul) from Steck et al. (1993) and Tso Kar area (Epard and Steck, 2008). N-T = Nyimaling-Tso Morari gneiss dome.

Figure 4. Parameter maps for evaluating morphology and erosion in the Zanskar River basin. (A) TRMM mean annual rainfall distribution map illustrating the precipitation gradient from west to east. Rainfall map was created using the 1998–2009 TRMM time series for mean annual rainfall; (B) Mean slope for the Zanskar River basin calculating using a 1-km radius circular moving window; (C) Local 5-km relief expressed as the difference between maximum and minimum elevation in a given area of a 5-km radius circular moving window; (D) Normalized channel steepness index (k_{sn}) calculated using TopoToolbox 2.0 (Schwanghart and Scherler, 2014). Subcatchments within the Zanskar River basin are outlined in gray in Figs. 2A-C.

Figure 5. Longitudinal profiles for tributaries of the Zanskar River. (A) Raw channel profiles were smoothed using a 2 km radius moving average window to remove elevation spikes. Black dashed lines mark trunk river tributaries; light gray dotted lines mark minor tributaries to Tsarap River catchment. Arrows indicate published locations of recessional moraines (Burbank and Fort, 1985; Damm, 2006; Mitchell et al., 1999; Owen and Benn, 2005); (B) Mean normalized channel steepness index (k_{sn}) values plotted for every 2 km segment along river longitudinal

profiles for all main streams. Values were extracted using MATLAB code adapted from TopoToolbox 2.0 (Schwanghart and Scherler, 2014).Abbreviations for streams are: K = Khurna; M = Markha; O = Oma Chu; S = Stod;; T = Tsarap; TC = Tsarap Chu; TZ = Toze Lungpa; and Y = Yunam.

Figure 6. Bulk petrographic compositions of Zanskar sediments. (A) Bulk compositions classified by Q (quartz), F (feldspathic), and L (lithic) framework grains following the Gazzi-Dickinson method of point counting (Ingersoll et al., 1984) and classified after Garzanti and Vezzoli (2003). Gray lines indicate data corrections for Source Rock Density (SRD; Vermeesch et al., (in press). Open diamonds are petrographic data from the lower Zanskar Gorge, where Z = Zanskar-Indus confluence and M = Markha River (Blöthe et al., 2014); (B) Bulk composition of Zanskar sediments plotted onto the (garnet + kyanite + sillimanite) – pyroxene – (zircon + tourmaline + rutile + amphibole + epidote) ternary diagram. Fields for Greater Himalaya "Formation I" kyanite- and fibrolite-bearing gneiss, Tethyan and Lesser Himalaya drawn after Garzanti et al. (2007). Samples are numbered after Table 1.

Figure 7. Bulk major element geochemistry of Zanskar River sediments plotted on the ternary Al_2O_3-CaO+Na_2O-K_2O diagram (Fedo et al., 1995) with Chemical Index of Alteration (CIA) values (Nesbitt et al., 1980). Mineral abbreviations are as follows: bt = biotite; chl = chlorite; gb = gibbsite; il = illite; kao = kaolinite; ksp = potassium feldspar; m = muscovite; pl = plagioclase; sm = smectite. Samples for average Archean upper crust (gray square), average granodiorite (open square), average granite (open diamond), and average A-type granite (gray diamond) are shown (Anderson and Bender, 1989; Condie, 1993; Winter, 2010). Line indicates typical

weathering evolution path for bedrock unaffected by K-metasomatism (Fedo et al., 1995). Samples are numbered after Table 1.

Figure 8. Crossplot of ε_{Nd} and $^{87}Sr/^{86}Sr$ compositions for Zanskar River sediments compared to other bedrock data from the Panjal Traps (Shellnutt et al., 2012; Shellnutt et al., 2014), the Greater and Lesser Himalaya (Ahmad et al., 2000; Deniel et al., 1987; Inger and Harris, 1993; Parrish and Hodges, 1996), Transhimalaya (Rolland et al., 2002), and additional Tethyan Himalaya (diamonds) and Greater Himalaya (squares) (Richards et al., 2005) from the Sutlej River. Samples are numbered after Table 1.

Figure 9. Diagram showing the progressive downstream variation in bulk sediment (A) $^{87}Sr/^{86}Sr$ and (B) ε_{Nd} compositions for the Zanskar River. Error bars are smaller than symbol size for propagated Sr and ε_{Nd} errors. Samples are numbered after Table 1.

Figure 10. KDE diagrams of U-Pb zircon ages from Zanskar River sediments.

Figure 11. Schematic diagram illustrating detrital framework grain and detrital zircon populations of Zanskar sands. Q = quartz; F = feldspars; Lc = lithic carbonate; Lsm = other sedimentary and low-rank metasedimentary; Lm = medium- to high-rank metamorphic; and Lv = volcanic and metavolcanic. Rank of metamorphic grains and MI index (0–500; Garzanti and Vezzoli (2003). Concentrations of Zr >> 300 ppm may indicate hydraulic sorting and enrichment of sample in dense phases. Black line denotes trunk Zanskar River, with gray lines for tributaries. Samples are numbered after Table 1.

Figure 12. Multidimensional scaling (MDS) plots showing the Kolmogorov-Smirnov distances between Zanskar River sediments and selected bedrock. (A) Classical MDS plot of bulk major element geochemistry data; (B) Nonmetric MDS plot of SRD-corrected bulk petrographic data; (C) Nonmetric MDS of Zanskar River detrital zircon U-Pb ages; and (D) Nonmetric MDS of selected Himalaya bedrock and Zanskar River detrital zircon U-Pb ages. Regional Himalayan U-Pb zircon data are same as Figure S2. Samples are numbered after Table 1. Data were plotted using R code 'provenance' written by Vermeesch et al. (2016). Solid lines indicate closest neighbor and dashed lines near neighbors in similarity calculations. Bedrock abbreviations in Fig. 12D mostly follow depositional ages: pЄ-Є = Proterozoic to Cambrian; D-O = Devonian to Ordovician; M-P = Mississippian to Permian; T-J = Triassic to Jurassic; LK = lower Cretaceous; uK-Pg = upper Cretaceous to Paleogene; and ZGH = Zanskar Greater Himalayan bedrock (Horton and Leech, 2013).

Figure S1. KDE diagrams for selected bedrock U-Pb data for the Zanskar River Basin. Selected samples are from the Indus and Tar Groups (Henderson et al., 2010; Wu et al., 2007), Zanskar region Greater Himalaya (Horton and Leech, 2013), Panjal Traps (Shellnutt et al., 2011), and Cambro-Ordovician granites in Zanskar and the NW Himalaya (Cawood et al., 2007; Girard and Bussy, 1999; Kwatra et al., 1999; Miller et al., 2001; Pognante et al., 1990). Selected bedrock ages for southern Tethyan Himalaya, Greater Himalaya, and correlative strata from the eastern and central Himalaya were plotted (in gray) according to depositional age and compiled into composite KDE diagrams (Clift et al., 2014; DeCelles et al., 2000; Gehrels et al., 2011; Hu et al., 2015; Hu et al., 2012; McQuarrie et al., 2008; Myrow et al., 2010; Myrow et al., 2003).

TABLES

Table 1. Sample locations for Zanskar River sediments.

Table 2. Bulk petrography of Zanskar River sediments.

Table 3. Major and trace element geochemistry of Zanskar River sediments.

Table 4. Nd and Sr isotope geochemistry of Zanskar River sediments.

Table S1. U-Pb zircon ages of Zanskar River sediments.

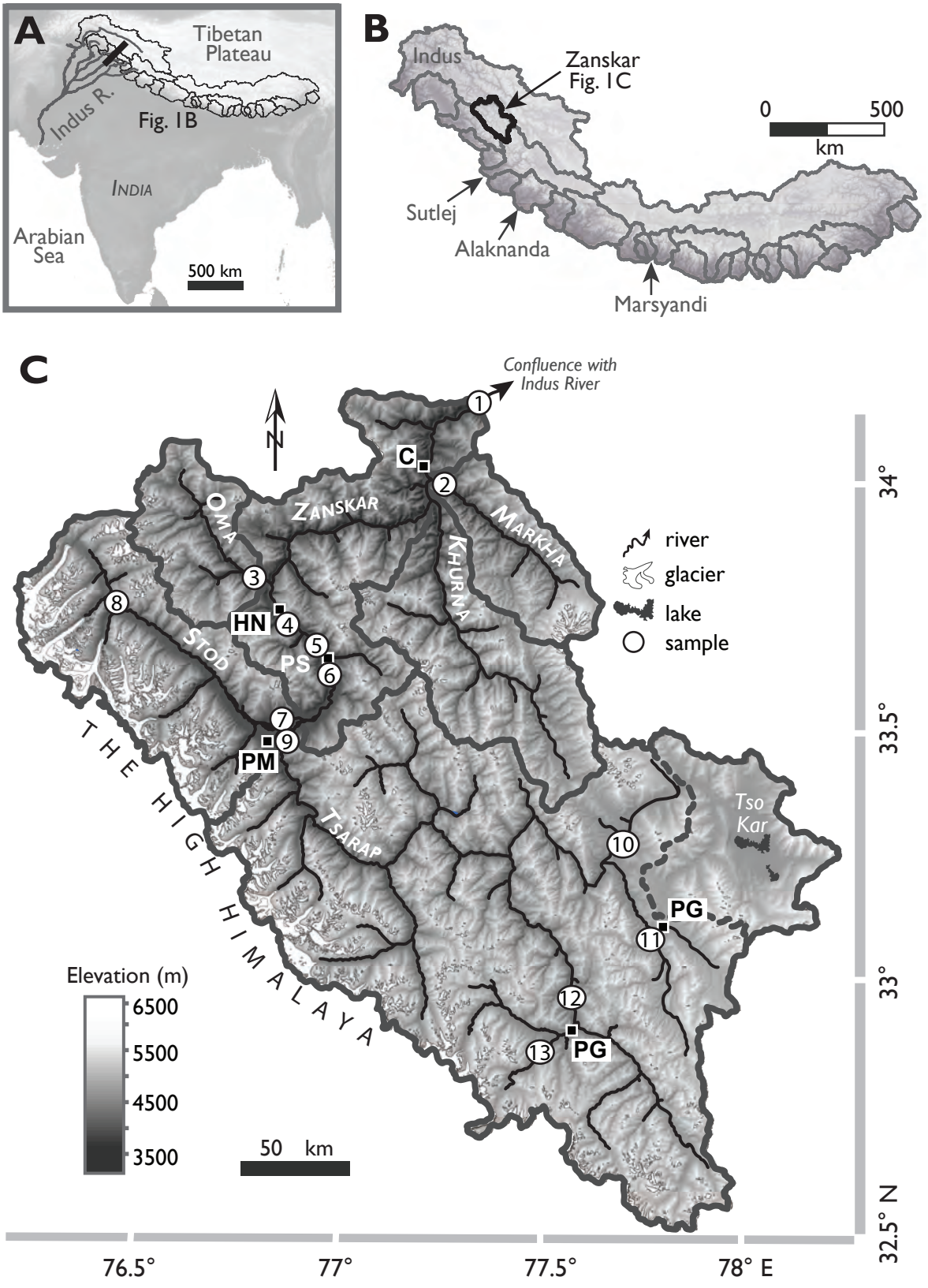
A
Tibetan Plateau
Indus R.
Fig. 1B
INDIA
Arabian Sea
500 km
B
Indus
Zanskar
Fig. 1C
0
500
km
Sutlej
Alaknanda
Marsyandi
C
Confluence with Indus River
N
ZANSKAR
OMA
KHURNA
MARKHA
STOD
HN
PS
PM
THE HIGH HIMALAYA
TSARAP
Tso Kar
PG
PG
river
glacier
lake
sample
Elevation (m)
6500
5500
4500
3500
50 km
34°
33.5°
33°
32.5° N
76.5°
77°
77.5°
78° E

Figure 1

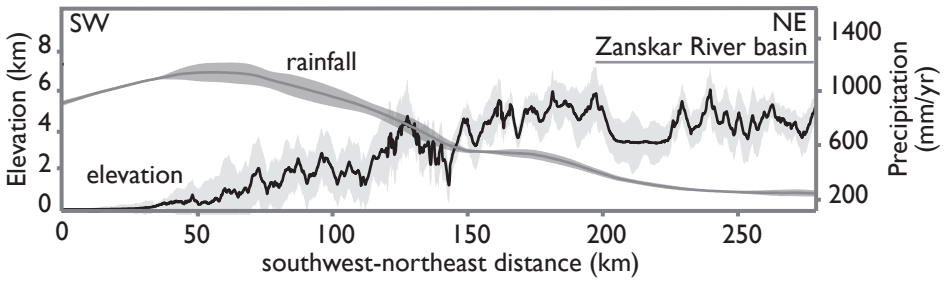
SW
NE
Zanskar River basin
rainfall
elevation
Elevation (km)
Precipitation (mm/yr)
0
2
4
6
8
200
600
1000
1400
0
50
100
150
200
250
southwest-northeast distance (km)

Figure 2

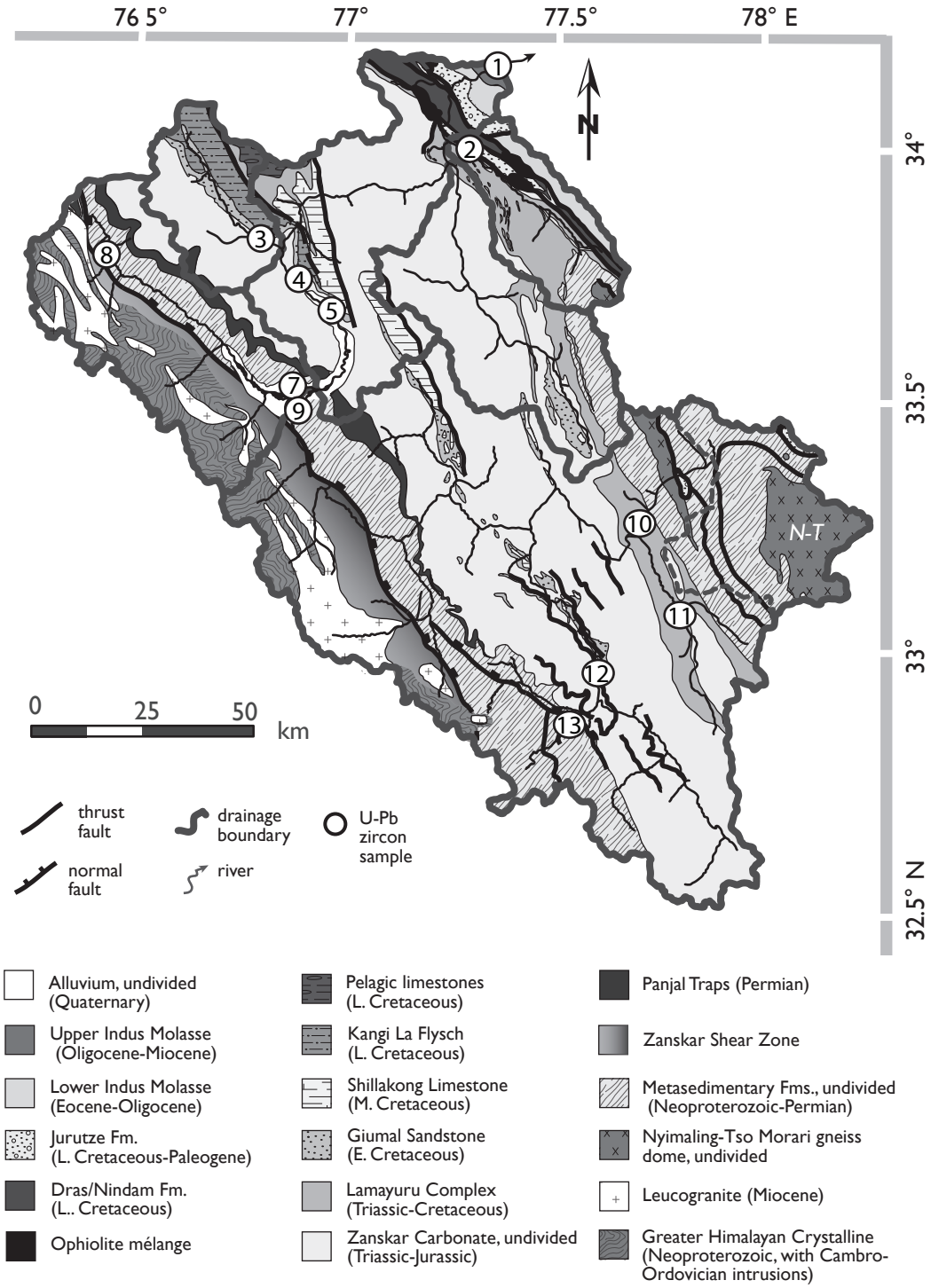
76 5°
77°
77.5°
78° E
34°
33.5°
33°
32.5° N
N
1
2
3
4
5
7
8
9
10
11
12
13
N-T
0
25
50
km
thrust fault
normal fault
drainage boundary
river
U-Pb zircon sample
Alluvium, undivided (Quaternary)
Upper Indus Molasse (Oligocene-Miocene)
Lower Indus Molasse (Eocene-Oligocene)
Jurutze Fm. (L. Cretaceous-Paleogene)
Dras/Nindam Fm. (L.. Cretaceous)
Ophiolite mélange
Pelagic limestones (L. Cretaceous)
Kangi La Flysch (L. Cretaceous)
Shillakong Limestone (M. Cretaceous)
Giumal Sandstone (E. Cretaceous)
Lamayuru Complex (Triassic-Cretaceous)
Zanskar Carbonate, undivided (Triassic-Jurassic)
Panjal Traps (Permian)
Zanskar Shear Zone
Metasedimentary Fms., undivided (Neoproterozoic-Permian)
Nyimaling-Tso Morari gneiss dome, undivided
Leucogranite (Miocene)
Greater Himalayan Crystalline (Neoproterozoic, with Cambro-Ordovician intrusions)

Figure 3

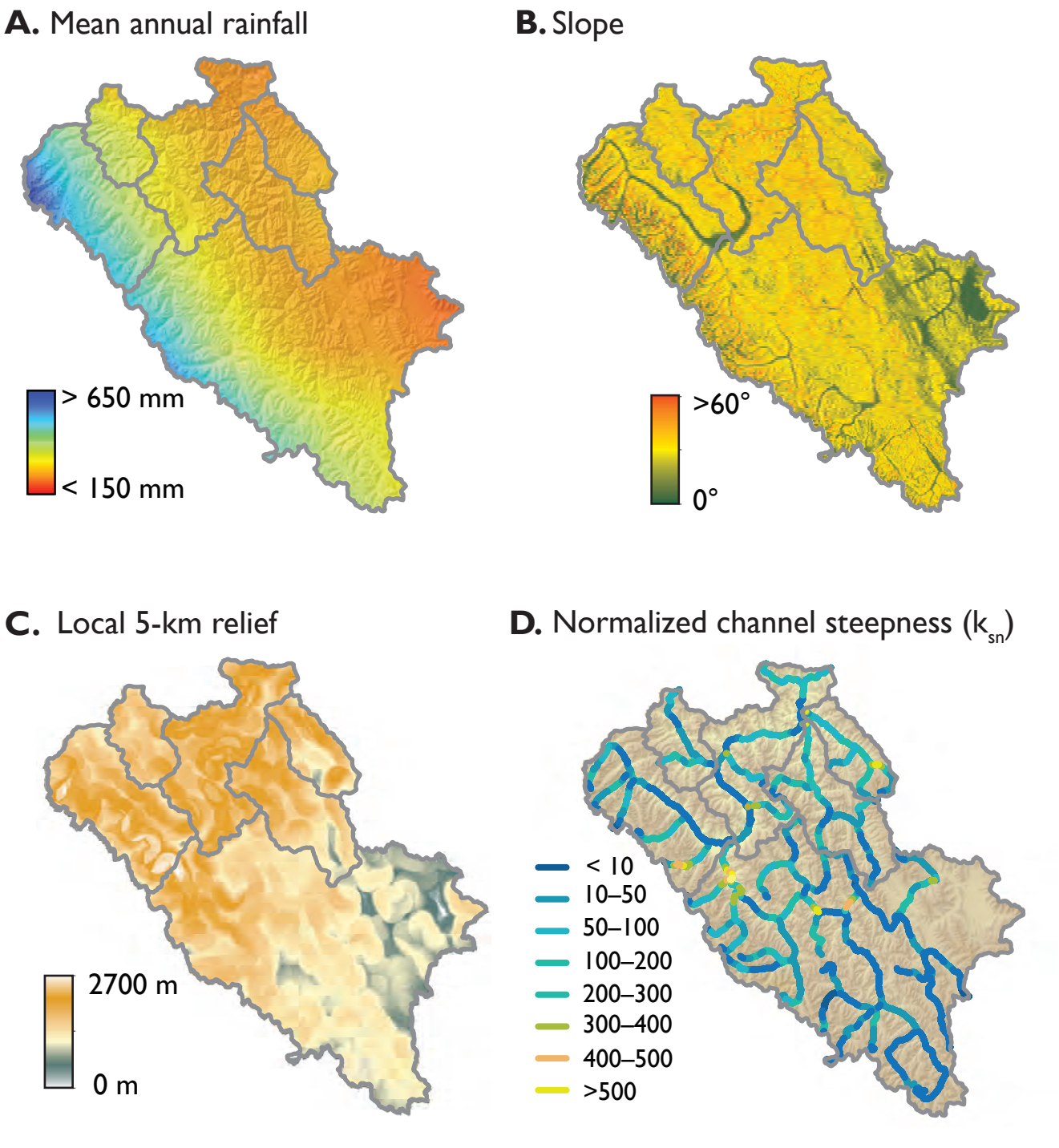
A. Mean annual rainfall
> 650 mm
< 150 mm
B. Slope
>60°
0°
C. Local 5-km relief
2700 m
0 m
D. Normalized channel steepness (k_{sn})
< 10
10–50
50–100
100–200
200–300
300–400
400–500
>500

Figure 4

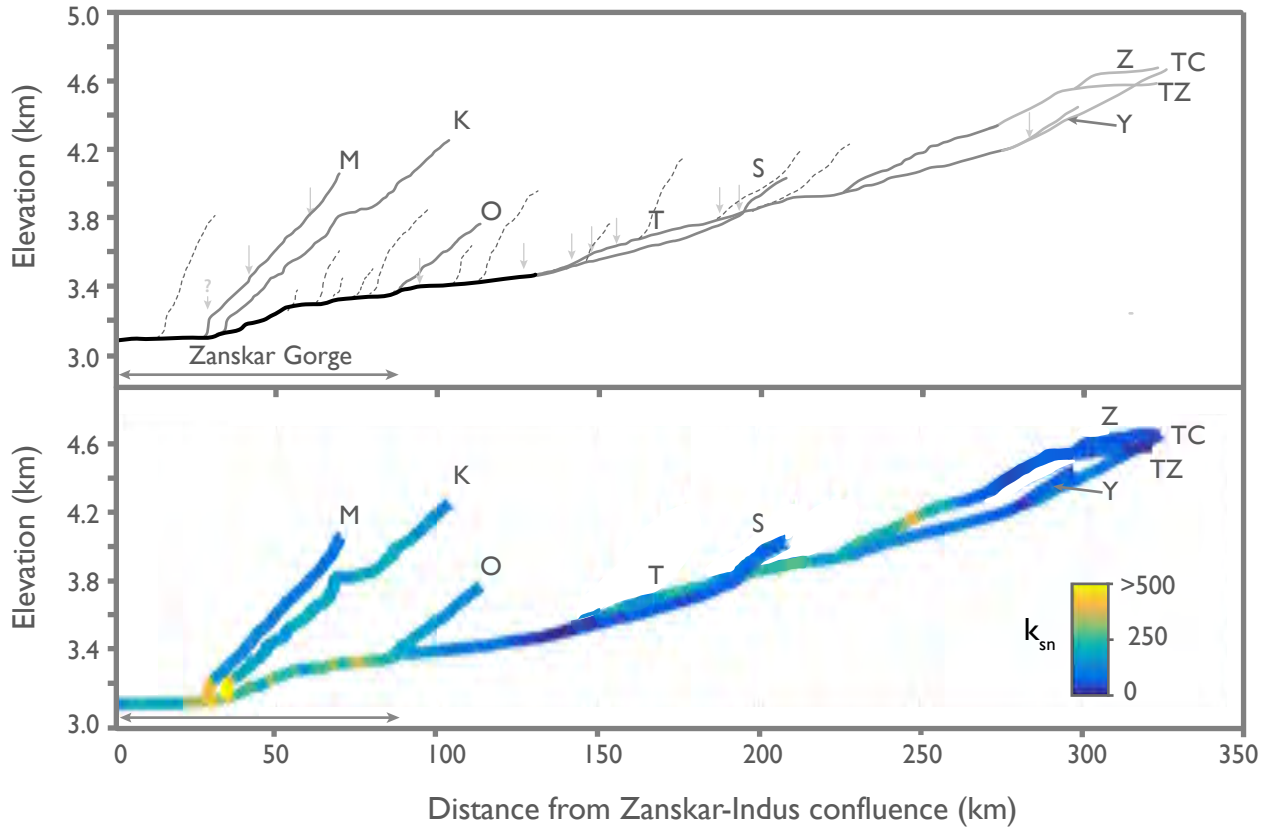
Elevation (km)
5.0
4.6
4.2
3.8
3.4
3.0
Zanskar Gorge
K
M
O
T
S
Z
TC
TZ
Y
Elevation (km)
>500
250
0
k_{sn}
0
50
100
150
200
250
300
350
Distance from Zanskar-Indus confluence (km)

Figure 5

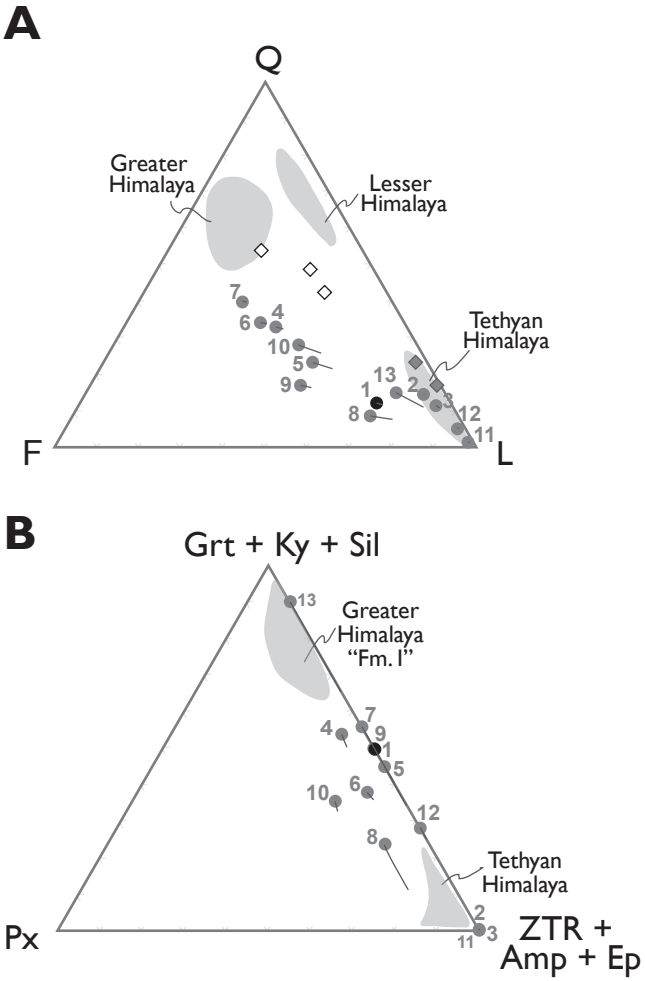
A
Q
Greater Himalaya
Lesser Himalaya
Tethyan Himalaya
F
L
B
Grt + Ky + Sil
Greater Himalaya "Fm. I"
Tethyan Himalaya
Px
ZTR + Amp + Ep

Figure 6

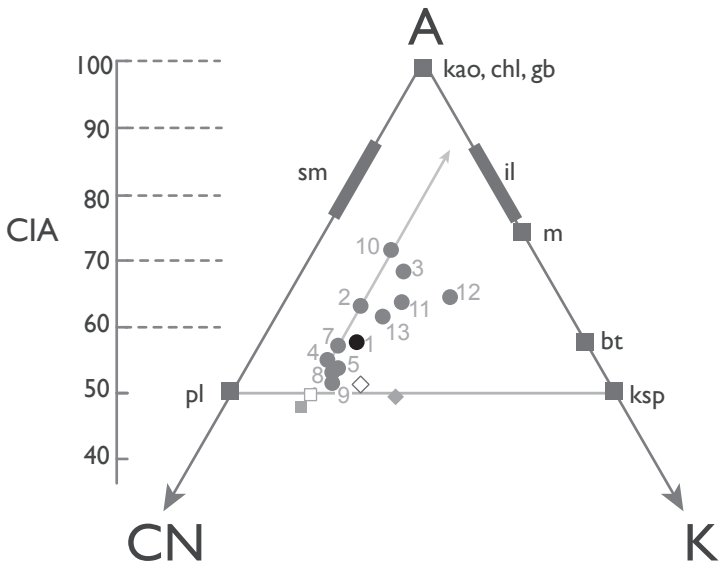
A
kao, chl, gb
sm
il
m
bt
ksp
pl
CN
K
CIA
100
90
80
70
60
50
40
1
2
3
4
5
7
8
9
10
11
12
13

Figure 7

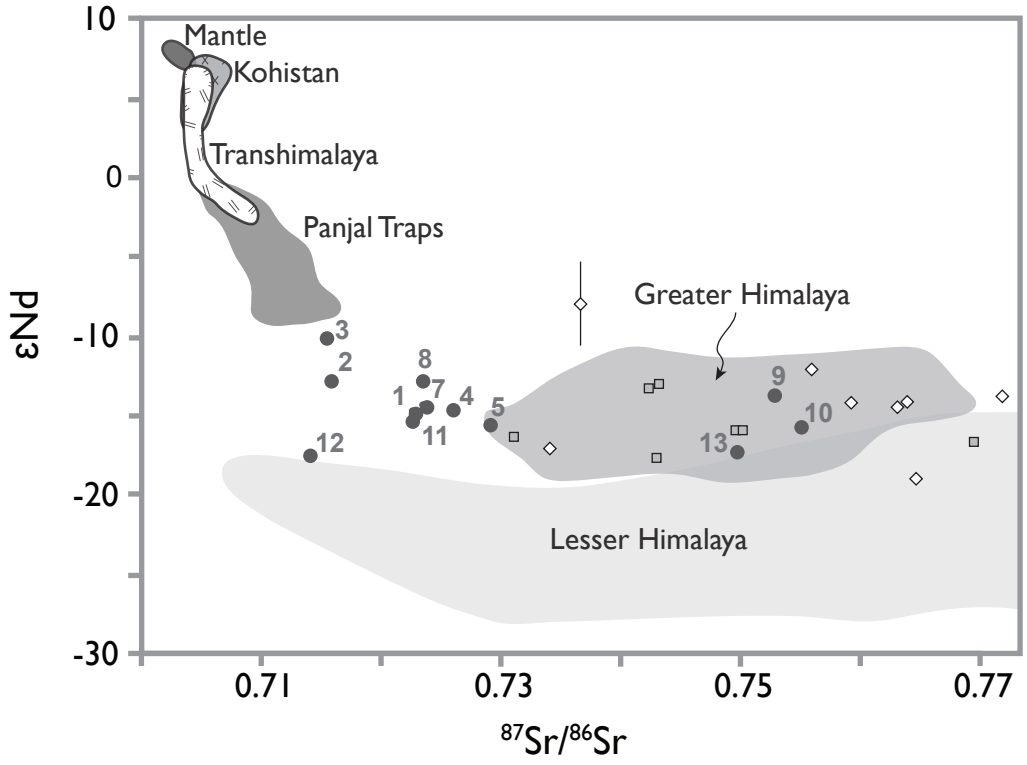

Figure 8
Jonell et al.

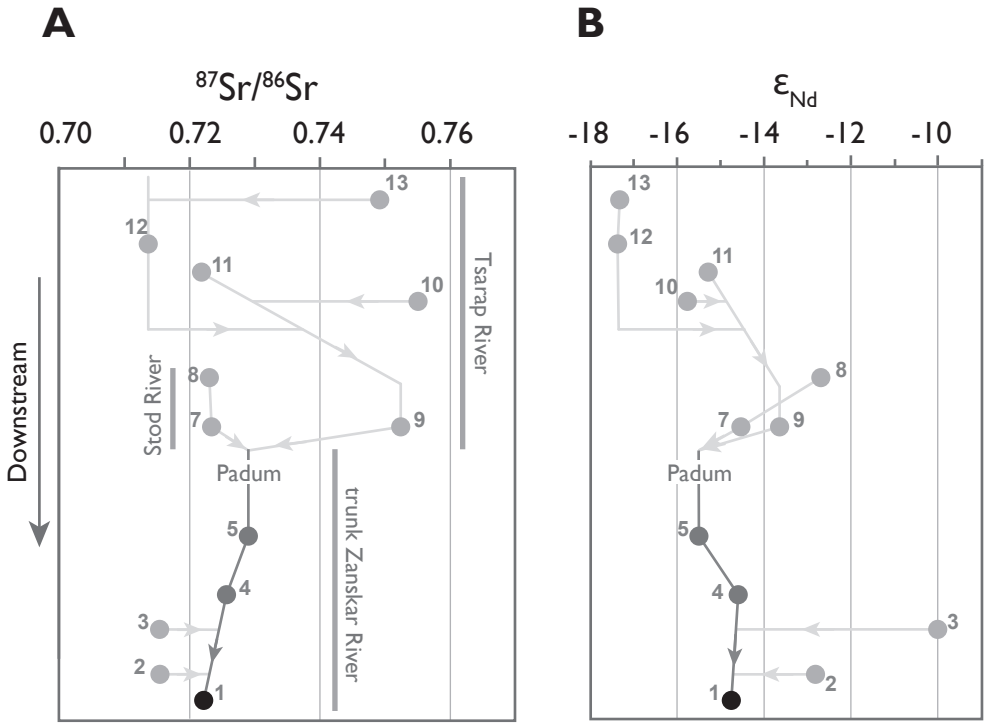
A
B
$^{87}Sr/^{86}Sr$
0.70
0.72
0.74
0.76
ε_{Nd}
-18
-16
-14
-12
-10
Downstream
Stod River
Tsarap River
trunk Zanskar River
Padum
1
2
3
4
5
7
8
9
10
11
12
13

Figure 9

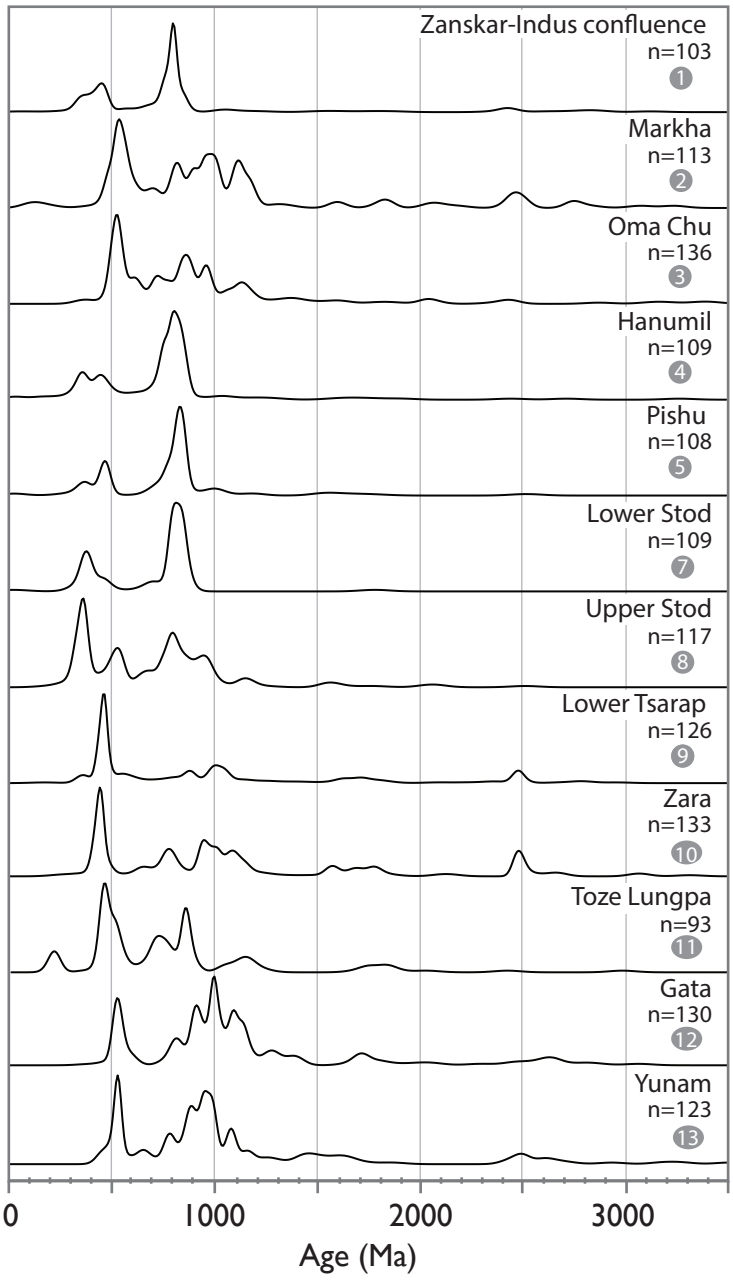
Zanskar-Indus confluence
n=103
1
Markha
n=113
2
Oma Chu
n=136
3
Hanumil
n=109
4
Pishu
n=108
5
Lower Stod
n=109
7
Upper Stod
n=117
8
Lower Tsarap
n=126
9
Zara
n=133
10
Toze Lungpa
n=93
11
Gata
n=130
12
Yunam
n=123
13
0
1000
2000
3000
Age (Ma)

Figure 10

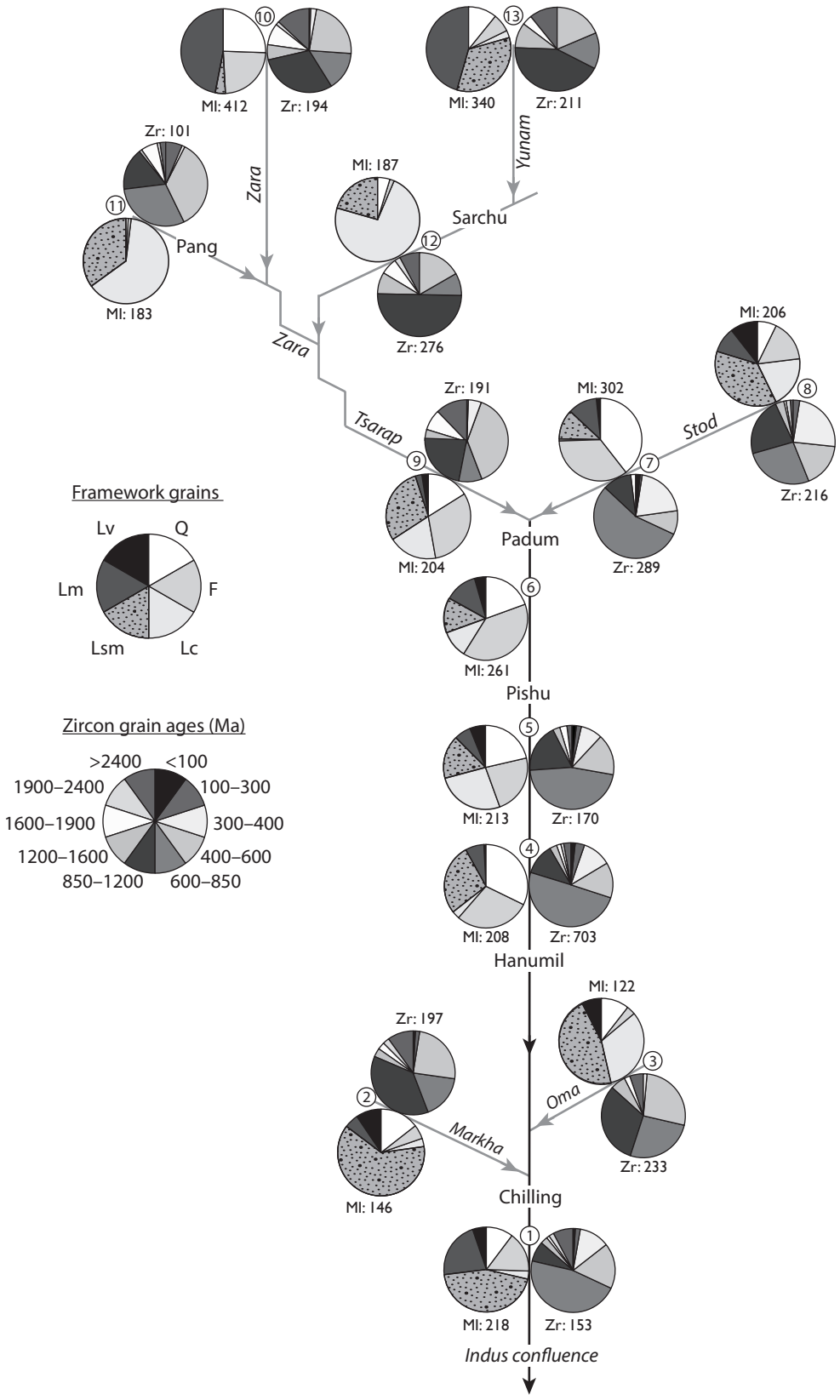
Framework grains
Lv
Q
Lm
F
Lsm
Lc
Zircon grain ages (Ma)
>2400
<100
1900–2400
100–300
1600–1900
300–400
1200–1600
400–600
850–1200
600–850
Ml: 412
Zr: 194
Ml: 340
Zr: 211
Zr: 101
Ml: 187
Zara
Yunam
Sarchu
Pang
Ml: 183
Zr: 276
Zara
Ml: 206
Zr: 191
Ml: 302
Tsarap
Stod
Zr: 216
Ml: 204
Zr: 289
Padum
Ml: 261
Pishu
Ml: 213
Zr: 170
Ml: 208
Zr: 703
Hanumil
Ml: 122
Zr: 197
Oma
Markha
Zr: 233
Ml: 146
Chilling
Ml: 218
Zr: 153
Indus confluence

Figure 11

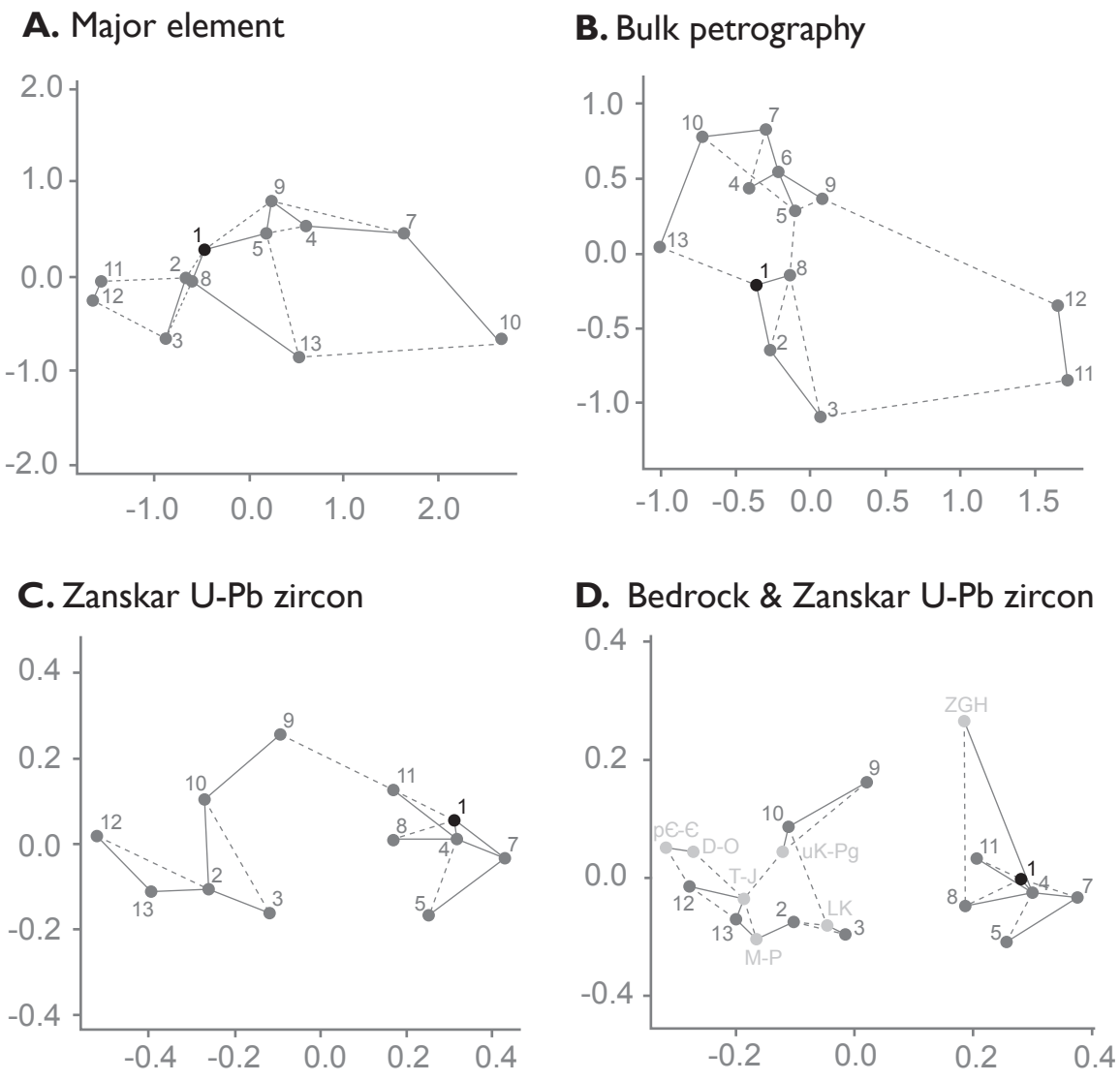
A. Major element
B. Bulk petrography
C. Zanskar U-Pb zircon
D. Bedrock & Zanskar U-Pb zircon
pЄ-Є
D-O
T-J
uK-Pg
LK
M-P
ZGH

Figure 12

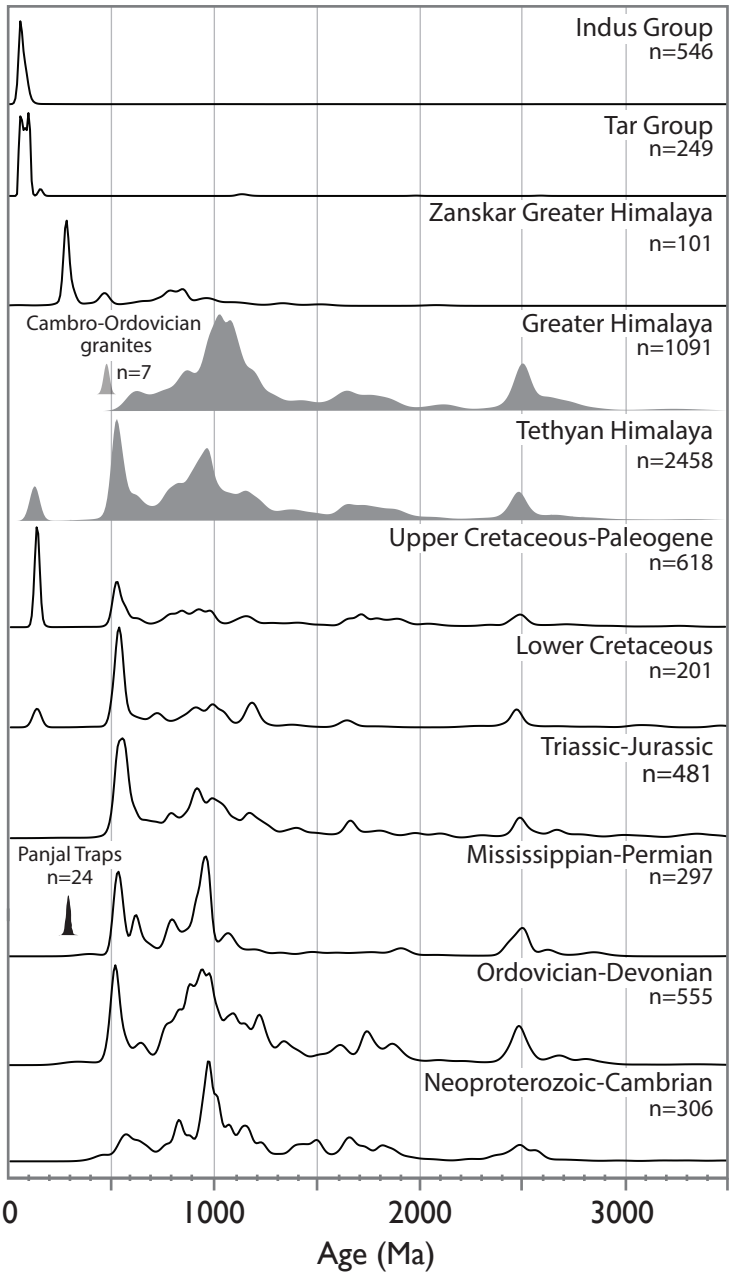
Indus Group
n=546
Tar Group
n=249
Zanskar Greater Himalaya
n=101
Cambro-Ordovician
granites
n=7
Greater Himalaya
n=1091
Tethyan Himalaya
n=2458
Upper Cretaceous-Paleogene
n=618
Lower Cretaceous
n=201
Triassic-Jurassic
n=481
Panjal Traps
n=24
Mississippian-Permian
n=297
Ordovician-Devonian
n=555
Neoproterozoic-Cambrian
n=306
0
1000
2000
3000
Age (Ma)

Figure S1